

Advanced finite element approaches for the 2D analysis of multilayered composite and sandwich beams

*Original*

Advanced finite element approaches for the 2D analysis of multilayered composite and sandwich beams / Sorrenti, Matteo; Turon, Francesc; Otero, Fermin; Martinez, Xavier; Gherlone, Marco. - In: EUROPEAN JOURNAL OF MECHANICS. A, SOLIDS. - ISSN 0997-7538. - ELETTRONICO. - 111:(2025), pp. 1-16.  
[10.1016/j.euromechsol.2025.105606]

*Availability:*

This version is available at: 11583/2997561 since: 2025-02-17T14:32:37Z

*Publisher:*

Elsevier

*Published*

DOI:10.1016/j.euromechsol.2025.105606

*Terms of use:*

This article is made available under terms and conditions as specified in the corresponding bibliographic description in the repository

*Publisher copyright*

(Article begins on next page)



Full length article

## Advanced finite element approaches for the 2D analysis of multilayered composite and sandwich beams

Matteo Sorrenti <sup>a</sup>, <sup>\*</sup>, Francesc Turon <sup>b</sup>, Fermin Otero <sup>b,c</sup>, Xavier Martinez <sup>b,c</sup>, Marco Gherlone <sup>a</sup>

<sup>a</sup> Department of Mechanical and Aerospace Engineering – Politecnico di Torino, Corso Duca degli Abruzzi 24, Torino, 10129, Italy

<sup>b</sup> International Centre for Numerical Methods in Engineering (CIMNE), Campus Nord UPC Edifici C2, Barcelona, 08034, Spain

<sup>c</sup> Department of Nautical Science and Engineering (CEN), Barcelona School of Nautical Studies (FNB), Technical University of Catalonia, BarcelonaTech (UPC), Pla de Palau 18, Barcelona, 08003, Spain

### ARTICLE INFO

#### Keywords:

Finite element method  
Refined Zigzag Theory  
Multi-scale  
Homogenization  
Reduced-order models  
Multilayered beams  
Sandwich structures

### ABSTRACT

This work presents a new critical overview and a numerical assessment of some advanced Finite Element (FE) approaches for the analysis of multilayered composite and sandwich beams. Firstly, the fundamental hypotheses behind the Timoshenko Beam Theory (TBT) and the Refined Zigzag Theory (RZT) are addressed, and corresponding low-order simple and efficient  $C^0$  two-noded beam elements are recalled for 2D cylindrical bending problems. Additionally, two novel advanced FE techniques are employed for 2D bending analysis, i.e. the Multi-Scale (MS) analysis and the Beam-Like Reduced Order Model (BLROM). The proposed FE models are used to investigate the static cylindrical bending response of multilayered composite and sandwich beams under different boundary conditions. The results demonstrate the superior predictive capabilities of the RZT, MS and BLROM models compared to the TBT one. Furthermore, despite having the same kinematics as the TBT, the MS and BLROM models guarantee enhancements in axial strain and transverse shear stress distributions. In addition, the RZT confirms its superior accuracy in predicting both transverse displacements and strains across the laminate thickness. Depending on their accuracy, the RZT, MS and BLROM models are computationally more advantageous than other expensive high-fidelity FE approaches and excellent candidates for the 2D static analysis of multilayered beams.

### 1. Introduction

In the last decades, multilayered composite and sandwich structures have been widely used in many engineering fields (aerospace, marine, civil, automotive and military) thanks to their attractive specific properties, such as high strength-to-weight ratio and good fatigue behaviour. However, during the structural design processes, particular attention should be paid to their transverse normal and shear deformability. In fact, their material mechanical properties change in the transverse through-the-thickness direction. This layer arrangement, generally, leads to a more pronounced transverse anisotropy that complicates the structural response and might cause interlaminar catastrophic failures, such as debonding and delamination. Therefore, researchers and engineers require sufficiently accurate models in order to predict correctly the response of multilayered composite and sandwich structures.

In the literature, the analytical exact three-dimensional solution is available only for a few cases. For instance, in Pagano (Pagano, 1969, 1970a), the exact elasticity solutions for simply supported cross-ply and

sandwich multilayered composite plates under sinusoidal transverse pressure have been provided. Similarly, the solution for cylindrical bending of simply supported angle-ply laminated plates has been reported (Pagano, 1970b). Moreover, Noor and Burton (1990) and Savoia and Reddy (1992) through different approaches, have obtained a set of analytical exact solutions for vibration and bending problems of simply-supported anti-symmetric angle-ply laminates.

The provided examples highlight the difficulty of obtaining an analytical three-dimensional solution for more general cases. In fact, only simple problems can be investigated, i.e. simply-supported boundary conditions and sinusoidal or uniform load pressures. These limitations restrict the practical applicability of these three-dimensional models.

In the last decades, many researchers have formulated approximated structural models as valid alternatives to overcome the previous limitations. In such models, the displacement field is assumed a-priori according to some kinematic hypotheses. Among the displacement-based theories, in the Equivalent Single Layer (ESL) models, the displacement field is assumed as a function of a limited number of

\* Corresponding author.

E-mail address: [matteo.sorrenti@polito.it](mailto:matteo.sorrenti@polito.it) (M. Sorrenti).

kinematic variables and for the whole laminate thickness. With particular reference to beam applications, the most used theories are the Bernoulli–Euler (EB), the Timoshenko (TBT) (Timoshenko and Woinowsky-Krieger, 1959) and the Reddy’s Third-order Shear Deformation Theory (Reddy’s TSDT) (Reddy, 1984). Based on different kinematic assumptions, these theories are able to accurately predict the global behaviour, such as maximum displacements, natural frequencies and buckling loads, of a wide range of beam structures.

In the EB beam theory, the effect of transverse shear deformability is neglected, limiting the applicability to slender beam structures. The TBT includes the transverse shear deformability as a constant through-the-thickness distribution, whereas Reddy’s TSDT assumes a cubic variation of the in-plane displacements, allowing a parabolic transverse shear stress distribution compatible with the three-dimensional elasticity. However, these models are quite inaccurate in the local through-the-thickness predictions of the in-plane displacements and stresses of multilayered composite structures. In fact, changes in the slopes of axial displacements and strains across the lamina interfaces, as well as more complex transverse shear stress distributions, cannot be predicted correctly.

A better approximation of the transverse shear stress can be achieved using the *a-posteriori* technique of integrating the local equilibrium equations, aka Cauchy’s equations. The interested reader is addressed for a complete survey on the existing ESL models to the review work of Abrate and Di Sciuva (2017).

The Layer-Wise (LW) theories represent a valid alternative to exploring in a more accurate way the structural response of multilayered structures. In fact, the advantage of these models relies on the layer-by-layer independent assumption of the displacement field, which better represents the three-dimensional behaviour. Clearly, the computational cost of these models is directly dependent on the number of layers, and they are generally more expensive than the ESL theories. However, their good accuracy in displacement and stress predictions makes them interesting in Finite Element (FE) applications, as reported in Refs. Carrera (2003), Demasi (2008).

In the last decades, the ZigZag Theories (ZZTs) have been proposed for the study of multilayered structures. The ZZTs are generally formulated using a limited number of unknown kinematic variables, such as ESL theories, but the displacement field is enriched with a local refinement given by the zigzag functions. The zigzag kinematics is a crucial point of the resulting model accuracy. In the literature, many authors have developed different approaches to characterize the zigzag local contribution for the analysis of multilayered structures. Among the existing approaches, it is worth mentioning the Murakami’s model (Murakami, 1986), which uses geometrically-based zigzag functions are well suited only for periodic laminates, and Di Sciuva’s model (Di Sciuva, 1986), which implements physically-based zigzag functions by enforcing the transverse shear stress continuity at the layer interfaces. The advantage in the model’s accuracy of Di Sciuva’s zigzag functions over Murakami’s relies on their link with the transverse shear mechanical properties and layer thickness geometry. However, Di Sciuva’s zigzag model suffered from inconsistencies in the correct representation of the transverse shear stress at the clamped edges, and the  $C^1$ -continuity requirement made it computationally more expensive than other models for FE formulations.

The recently developed Refined Zigzag Theory (RZT) (Tessler et al., 2007) has been used to investigate various multilayered composite and sandwich structures. The RZT kinematics is derived by combining the first-order global kinematics with a layer-wise contribution represented by piece-wise continuous linear zigzag functions that vanish at the bottom and top external surfaces. The zigzag slopes are characterized by a partial fulfilment of the transverse shear stress continuity at the layer interfaces, which makes their distributions constant with jumps across the interfaces. This finer description has been demonstrated to be very accurate in the global predictions for displacements, buckling loads and natural frequencies, as well as the local quantities, such

as in-plane displacements, axial strains and stresses (Tessler et al., 2007, 2010; Gherlone et al., 2011; Gherlone, 2013; Groh et al., 2015). Clearly, the transverse shear stresses computed through the constitutive relations are still discontinuous across the laminate thickness. However, the transverse shear deformability is correctly predicted, and the RZT does not require any shear correction factor. The *a-posteriori* integration of the local equilibrium equations recovers a continuous through-the-thickness distribution of the transverse shear stresses (Iurlaro et al., 2013). Examples in the current literature of applications of the RZT are the following ones. Hasim (2018) has combined the RZT with the Iso-Geometric Analysis (IGA) for the static analysis of multilayered composite beams. Dorduncu (2019) has solved the RZT equilibrium equations for highly heterogeneous beams via the Peridynamic Differential Operator. Ascione and co-workers (Ascione and Gherlone, 2018; Ascione et al., 2020, 2022) have investigated the stability behaviour and critical buckling loads of multilayered beams embedded with piezoelectric materials. Recently, Malekimoghadam et al. (2023) have considered the RZT for the analysis of composite beams integrated with carbon nanotubes, and Kefal et al. (2021) have experimentally applied the RZT for shape-sensing applications on sandwich beams. Although the provided RZT references do not cover all the aspects of the RZT results, they just want to give an overview of the wide range of applicability of this recent zigzag model.

In the FE modelling, the RZT requires only the  $C^0$ -continuity for the shape functions selection, thus, simple and efficient finite elements can be easily formulated, as done in Gherlone et al. (2011), Oñate et al. (2012) and Di Sciuva et al. (2015). The results provided by Refs. Gherlone et al. (2011), Oñate et al. (2012), Di Sciuva et al. (2015) demonstrated the accuracy of RZT in predicting the structural response for laminated beams. However, without adopting mixed variational formulations, see Refs. Tessler (2015), Groh and Weaver (2015), the shear stress recovery procedure cannot be adopted for low-order beam finite elements. In this perspective, other mixed FE methodologies that tackle both global beam behaviour and local section deformations can be addressed.

Two mixed approaches, both characterized by describing the beam behaviour with a detailed 2D representation of its longitudinal section, are addressed in this study. Such representations are featured by reproducing the geometry and material characteristics that form the cross-section investigated beams with a high level of detail, which makes these techniques suitable for the study, either of layered sections or made with heterogeneous materials. Thanks to their representations, it is sought to establish a relationship between a state of deformation and the induced stress, i.e. at a constitutive level, or a relationship between the imposed displacement and the generated reaction, i.e. at a stiffness or rigidity level.

Specifically, this study covers the following two advanced FE techniques: the Multi-Scale (MS) analysis and the Beam-Like Reduced Order Models (BLROM) using Domain Decomposition (DD) and Mixing Dimensional Coupling (MDC). The MS analysis applied to beam models, distinguishes between two scales on the structure under investigation. These scales are separated by various orders of magnitude and are known as micro- and macro- scales. The macro one encloses the entire analysed structure, which is represented by the beam macro-model. The micro-scale model is meant to be small enough to capture the lamination or section physiognomy of the beams making up the macro-model. On this scale, the Representative Volume Elements (RVEs) are defined, which represent infinitesimal spans of the beams in the form of Plane-Stress (PS) models.

These RVEs are then characterized through a homogenization procedure, which aims to induce the strain states that are given on the macro-model and capture the resulting average stress state. The strain states are induced by defining kinematic Boundary Conditions (BC) at the borders of the RVE, giving rise to the so-called Boundary Value Problem (BVP) for which there are different solutions. Once the relationship between stresses and strains is obtained for each RVE in the

form of a constitutive tensor, it is then used in different regions of the macro-model. In a linear elastic analysis such as the one under consideration, this relationship is constant over time. Therefore, it is only necessary to homogenize the RVEs once at the beginning of the static analysis. Performing a Multi-Scale analysis in which the macro model is a beam model requires establishing a relationship between the possible strain states at their integration points and the kinematics of the RVE models defined at the microscale. There are numerous publications that address this subject and in which different kinematic theories are used. Among them, the interested reader is addressed to the studies carried out by Kouz and co-authors in Kouznetsova et al. (2004), Geers et al. (2007), Coenen et al. (2008) in which solid RVE or Plane Stress (PS) are defined for macro Reissner–Mindlin shell or TBT beam models, respectively. The aforementioned approach is adopted in the present paper to characterize the 2D laminar beam cross sections.

The second modelization technique taken into account relies on the definition of Reduced Order Models (ROMs) compatible with beam elements, i.e. with the same degrees of freedom, and their corresponding reactions (Monaghan et al., 2000). These ROMs are obtained from PS models representing spans of the beam structure under consideration. At their edges, two coupling interfaces are defined that relate the DOFs of these models to those of a beam element. In the present work, such coupling is performed based on the work equilibrium statement introduced by McCune et al. (2000). The advantage of these Beam-Like ROMs (BLROM) over conventional beam elements lies in the fact that the former is able to characterize the behaviour of beams with some type of discontinuity, unlike the latter, which can only be used for beams of constant section. In the literature, various works adopted this technique; among them, worth mentioning are Refs. Monaghan et al. (2000), Yu et al. (2012).

As a matter of fact, beam or shell finite elements are often used to study the structural response of multilayered composite and sandwich structures, and they are quite accurate if the hypotheses behind the structural theory formulation are respected. The mixed-modelling technique can represent a valid tool to enhance the productivity capabilities of the numerical model when more detailed displacement/stress descriptions are required without excessively increasing the computational cost.

Based on the previous literature overview and with the aim to better address the advantages and drawbacks of some advanced and recent FE approaches, in this paper, the linear static response of multilayered composite and sandwich beams is numerically assessed. More specifically, the Timoshenko Beam Theory (TBT), the Refined Zigzag Theory (RZT), the Multi-Scale (MS) analysis, and the Beam-Like Reduced Order Model (BLROM) are considered in this study for the bending 2D analysis of multilayered beams. In Section 2, each beam model's characteristics, finite element formulations and constitutive relations are presented in a concise manner, in order to give a simple and general overview of the most relevant properties. In Section 3, a detailed numerical assessment devoted to evaluating the accuracy and limitations of each model with respect to high-fidelity FE solutions is presented and discussed. Finally, in Section 4, some concluding remarks are presented based on the obtained numerical results of the selected advanced FE approaches. Moreover, possible future perspectives are outlined based on the major advantages and relative limitations of these approaches for the 2D cylindrical bending analysis of multilayered composite and sandwich beams.

## 2. Methodologies

In this Section, the general beam notations, model characteristics and element formulations are briefly recalled.

### 2.1. General 3D beam notation and preliminaries

Let us consider a general straight multilayered beam made of a finite number  $N$ , of perfectly bonded layers. Without loss of generality, this assumption has been made to evaluate the multilayered beam response only in the linear elastic regime. We denote with  $L$  its length,  $h$  is the total thickness and  $b$  its width, as shown in Fig. 1. The material points of the beam are referred to an orthogonal Cartesian coordinate system defined by the vector  $\mathbf{X} = \{x, y, z\}$ , where  $x$  represents the beam-axis coordinate,  $y$  and  $z$  represent the transverse coordinates. More specifically,  $z$  is the transverse coordinate along the thickness-wise direction, and  $y$  is the coordinate along the width direction. The origin of the beam reference frame is fixed in the range identified by  $x \in [0, L]$ ,  $y \in [-b/2, +b/2]$  and  $z \in [-h/2, +h/2]$ .

According to Fig. 1, let us denote: with the  $(k)$  superscript, the quantities corresponding to the  $k$ th layer ( $k = 1, 2, \dots, N$ ); with the  $(k)$  subscript, the quantities defined at the  $k$ th interface, i.e. between the  $k$ th and the  $(k + 1)$ th layers ( $k = 1, \dots, N - 1$ ). Thus, for the  $k$ th layer  $z \in [z_{(k)}, z_{(k+1)}]$ , with  $(k = 1, \dots, N)$ . Moreover, the subscripts  $B$  and  $T$  denote the bottom and top surfaces of the layer/beam.

Although a multilayered beam structure can be subjected to prescribed distributed loads,  $q(x)$ , as reported in Fig. 1, in this assessment, only prescribed displacements are considered.

The symbol  $(\bullet)_{,c}$  with  $c = x, y, z$  stands for the derivative of the quantity  $(\bullet)$  with respect to the  $x, y$  or  $z$  coordinate.

Finally, let us denote with  $\mathbf{d}(\mathbf{X})^T = [u_x(\mathbf{X}) \ u_y(\mathbf{X}) \ u_z(\mathbf{X})]$  the displacement vector of a point belonging to the beam in the  $(x, y, z)$  three-dimensional space, defined according to its orthogonal Cartesian coordinates.

### 2.2. Strain and stress relations in three-dimensional linear elasticity

Consistent with the 3D linear elasticity (Reddy, 2003), and under the assumptions of small displacements and rotations, the infinitesimal strain tensor, expressed in engineering notation, follows:

$$\begin{aligned} \epsilon_{xx}(\mathbf{X}) &= u_{x,x}(\mathbf{X}) \\ \epsilon_{yy}(\mathbf{X}) &= u_{y,y}(\mathbf{X}) \\ \epsilon_{zz}(\mathbf{X}) &= u_{z,z}(\mathbf{X}) \\ \gamma_{xz}(\mathbf{X}) &= u_{x,z}(\mathbf{X}) + u_{z,x}(\mathbf{X}) \\ \gamma_{yz}(\mathbf{X}) &= u_{y,z}(\mathbf{X}) + u_{z,y}(\mathbf{X}) \\ \gamma_{xy}(\mathbf{X}) &= u_{x,y}(\mathbf{X}) + u_{y,x}(\mathbf{X}) \end{aligned} \quad (1)$$

Taking into account that each material layer is linearly elastic and orthotropic, the generalized Hooke's law is written as follows:

$$\begin{Bmatrix} \sigma \\ \tau \end{Bmatrix}^{(k)} = \mathbf{C}^{(k)} \begin{Bmatrix} \epsilon \\ \gamma \end{Bmatrix}^{(k)} \quad (2)$$

where the  $C_{ij}^{(k)}$ ,  $i, j = 1, \dots, 6$  are the stiffness coefficients of the  $k$ th layer, see for instance (Reddy, 2003). The material stiffness  $\mathbf{C}^{(k)}$  matrix given by Eq. (2) for the  $k$ th layer, generally valid for any multilayered structure, includes in its expression (see Ref. Reddy (2003)) the effect of the rotation of the layer around the  $z$  axis. Hereafter, this angle (defined positive in the counterclockwise direction with respect to the  $x$ -axis) is denoted with the symbol  $Y^{(k)}$ . Furthermore, the  $C_{ij}^{(k)}$  coefficients are directly linked to the Young's ( $E_x, E_y, E_z$ ) and shear ( $G_{xy}, G_{xz}, G_{yz}$ ) moduli and Poisson's ratios ( $\nu_{ij}, i, j = x, y, z$ ). Moreover, the stress and strain quantities that appear in Eq. (2) are defined as follows:  $\sigma^T = [\sigma_{xx} \ \sigma_{yy} \ \sigma_{zz}]$ ,  $\tau^T = [\tau_{xz} \ \tau_{yz} \ \tau_{xy}]$  and  $\epsilon^T = [\epsilon_{xx} \ \epsilon_{yy} \ \epsilon_{zz}]$  and  $\gamma^T = [\gamma_{xz} \ \gamma_{yz} \ \gamma_{xy}]$ .

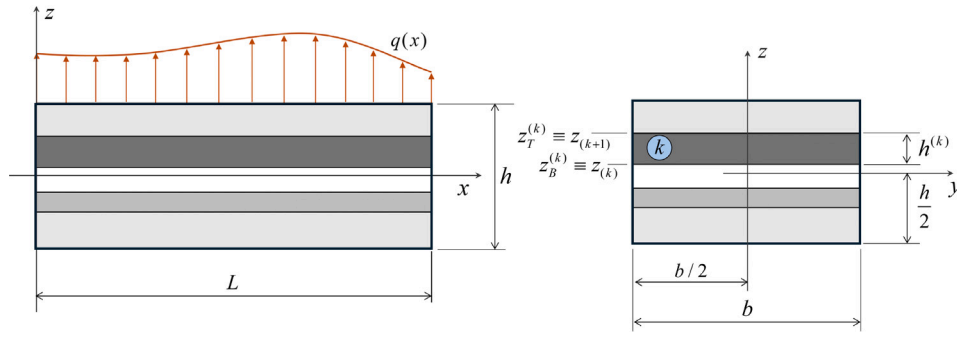


Fig. 1. General beam notation: beam geometry, coordinate system and loads.

### 2.3. The principle of virtual displacements

In this section, the Principle of Virtual Displacements (PVDs) is briefly recalled. Among the existing variational principles, Washizu (1975), the PVDs is the simplest principle used to obtain the equilibrium equations and the consistent boundary conditions. The same variational approach can be used to solve approximately the governing equation by implementing the FE method. The PVDs reads:

$$\int_V (\delta \epsilon^T(\mathbf{X}) \sigma(\mathbf{X}) + \delta \gamma^T(\mathbf{X}) \tau(\mathbf{X})) dV = \delta W_{ext} \quad (3)$$

where  $\delta$  is the virtual variation, and  $V$  is the volume of the beam.

Note that in Eq. (3), the expression for strains and stresses are theory/model dependent. If present,  $\delta W_{ext}$  is the virtual variation of applied external loads (concentrated forces and moments, distributed loads, etc.).

### 2.4. Timoshenko Beam Theory (TBT)

In this subsection, the kinematic assumptions and constitutive relations of the Timoshenko Beam Theory (TBT) are briefly recalled.

According to the TBT hypothesis (see Reddy (2003)), and assuming the beam deformation in the  $(x, z)$  plane, i.e. the cylindrical bending condition, the displacement field  $\mathbf{u} = \{u_x, u_z\}$  follows:

$$\begin{aligned} u_x(x, z) &= u(x) + z\theta(x) \\ u_z(x, z) &= w(x) \end{aligned} \quad (4)$$

where  $u(x)$  and  $w(x)$  are the uniform components of the axial and transverse displacement, respectively, and  $\theta(x)$  is the bending rotation around the positive direction of  $y$  axis. The kinematics of the Timoshenko beam model, as defined by Eq. (4), is shown in Fig. 2. From Eq. (1), the TBT strains read:

$$\begin{aligned} \epsilon_{xx}(x, z) &= u_{,x}(x) + z\theta_{,x}(x) \\ \gamma_{xz}(x, z) &= w_{,x}(x) + \theta(x) \end{aligned} \quad (5)$$

Moreover, taking into account the plane-stress behaviour, the stresses read:

$$\begin{aligned} \sigma_{xx}^{(k)}(x, z) &= E_x^{(k)} \epsilon_{xx}(x, z) \\ \tau_{xz}^{(k)}(x, z) &= G_{xz}^{(k)} \gamma_{xz}(x, z) \end{aligned} \quad (6)$$

where  $E_x^{(k)}$  and  $G_{xz}^{(k)}$  are the elastic and shear moduli for the  $k$ th lamina in geometric axis.

According to Eq. (6), the through-the-thickness transverse shear stress distribution is a piece-wise constant function with discontinuities at each interface, contrasting with the continuous and somewhat parabolic distribution in three-dimensional behaviour.

In order to match the global response with the elasticity results, a shear correction factor  $k_f$  is needed to modify the constitutive relations and the transverse shear stiffness.

Several methodologies are available in the literature for estimating this shear correction factor; among them, worthy of mention is the energy procedure described by Madabhushi-Raman and Davalos (1996)

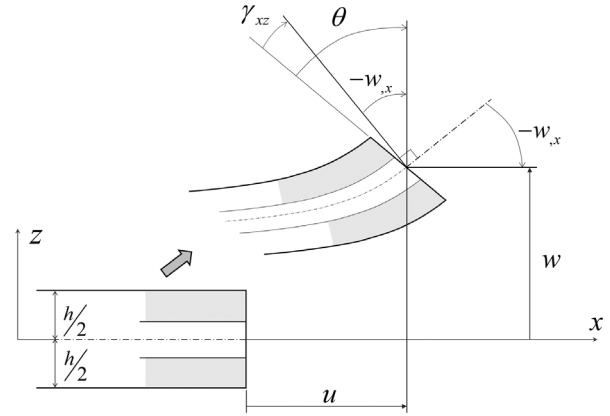


Fig. 2. Timoshenko beam model: geometry and kinematics notation.

and Oñate (2013).

Using the PVDs, i.e. Eq. (3), the TBT constitutive relations between force and moment resultants and strain components follows:

$$\begin{Bmatrix} N \\ M \\ T \end{Bmatrix} = \begin{bmatrix} A & B & 0 \\ B & D & 0 \\ 0 & 0 & k_f A_t \end{bmatrix} \begin{Bmatrix} u_{,x} \\ \theta_{,x} \\ w_{,x} + \theta \end{Bmatrix} = \mathbb{D} \begin{Bmatrix} u_{,x} \\ \theta_{,x} \\ w_{,x} + \theta \end{Bmatrix} \quad (7)$$

where  $N$  and  $T$  are the axial and transverse shear forces, and  $M$  the bending moment, respectively. Moreover,

$$\begin{aligned} A &= \int_h b E_x^{(k)} dz; \quad B = \int_h b z E_x^{(k)} dz; \\ D &= \int_h b z^2 E_x^{(k)} dz; \quad A_t = \int_h b G_{xz}^{(k)} dz \end{aligned} \quad (8)$$

Finally, within  $\mathbb{D}$ , it is possible to distinguish between the axial/bending stiffness  $\mathbb{D}_I$  and the shear stiffness  $\mathbb{D}_S$  being

$$\mathbb{D}_I = \begin{bmatrix} A & B \\ B & D \end{bmatrix} \quad \text{and} \quad \mathbb{D}_S = [k_f A_t]. \quad (9)$$

In FE approximation, the TBT requires only  $C^0$ -continuity for the choice of the shape function; thus, the simplest TBT-based element is a two-node element based on the linear Lagrangian polynomials. The complete formulation of these elements can be found in Oñate's book (Oñate, 2013).

### 2.5. Refined Zigzag Theory (RZT)

In this section, the basic assumptions of the Refined Zigzag Theory (RZT) for beams are recalled.

The RZT kinematics is described as a superposition of two displacement contributions: a Global (G) first-order one (which is continuous across to the beam thickness) and a Local (L) layer-wise correction of

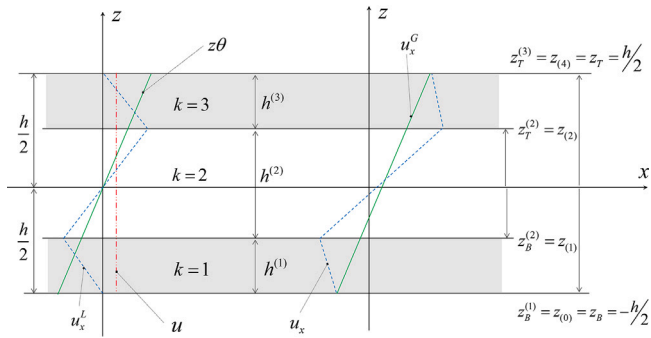


Fig. 3. Refined Zigzag kinematics for a three-layered beam: axial displacement contributions.

the axial displacements. The former is coincident with the Timoshenko model, whereas the latter is a continuous through-the-thickness piecewise function, with changes in their slopes between two adjacent layers.

According to the RZT (Di Sciuva et al., 2015) beam assumptions under the hypothesis of cylindrical bending condition, the displacement field reads:

$$\begin{aligned} u_x^{(k)}(x, z) &= u_x^G(x, z) + u_x^{L(k)}(x, z) \\ u_z^{(k)}(x, z) &= w(x, z) \end{aligned} \quad (10)$$

with

$$\begin{aligned} u_x^G(x, z) &= u(x) + z\theta(x) \\ u_x^{L(k)}(x, z) &= \phi^{(k)}(z)\psi(x) \end{aligned} \quad (11)$$

In Eqs. (10)–(11)  $u(x)$ ,  $w(x)$  are the uniform component of the axial and transverse displacements, respectively, and  $\theta(x)$  is the bending rotation. The  $\psi(x)$  represents the zigzag rotation of the through-the-thickness piecewise linear zigzag function, i.e.  $\phi^{(k)}(z)$ .

These zigzag functions are required to vanish on the top and bottom external surfaces of the beam, as shown in Fig. 3 for a three-layered symmetric beam.

For clarity, the final expression of the zigzag function is here reported; for more details, the interested reader is addressed to the Ref. Gherlone et al. (2011). Its final expression reads:

$$\phi^{(k)}(z) = (z + h/2)\beta^{(k)} + \sum_{q=1}^{k-1} h^{(q)}(\beta^{(q)} - \beta^{(k)}) \quad (12)$$

where  $\beta^{(k)} = \phi_{,z}^{(k)}$  is the zigzag slope obtained by the following expression:

$$\beta^{(k)} = \frac{G}{G_{xz}^{(k)}} - 1; G = h \left( \sum_{k=1}^N \frac{h^{(k)}}{G_{xz}^{(k)}} \right)^{-1} \quad (13)$$

Substituting Eqs. (10)–(13) into Eq. (1), the strain components read:

$$\begin{aligned} \epsilon_{xx}^{(k)}(x, z) &= u_{,x}(x) + z\theta_{,x}(x) + \phi^{(k)}(z)\psi_{,x}(x) \\ \gamma_{xz}^{(k)}(x, z) &= w_{,x}(x) + \theta(x) + \beta^{(k)}\psi(x) \end{aligned} \quad (14)$$

The stresses are expressed accordingly to the plane-stress constitutive relations valid for TBT, i.e. Eq. (6).

Using the PVDs, the constitutive relations of the RZT beam follow:

$$\begin{Bmatrix} N \\ M \\ M^\phi \\ T \\ T^\phi \end{Bmatrix} = \begin{bmatrix} A & B & A^\phi & 0 & 0 \\ B & D & B^\phi & 0 & 0 \\ A^\phi & B^\phi & D^\phi & 0 & 0 \\ 0 & 0 & 0 & A_t & B_t \\ 0 & 0 & 0 & B_t & D_t \end{bmatrix} \begin{Bmatrix} u_{,x} \\ \theta_{,x} \\ \psi_{,x} \\ w_{,x} + \theta \\ \psi \end{Bmatrix} \quad (15)$$

where  $N$  and  $T$  are the axial and transverse shear forces, and  $M$  the bending moment, respectively. In addition,  $M^\phi$  and  $T^\phi$  are, respectively, the bending moment and shear force associated with the zigzag effect.

Moreover,

$$\begin{aligned} A &= \int_h b E_x^{(k)} dz; B = \int_h bz E_x^{(k)} dz; D = \int_h bz^2 E_x^{(k)} dz; \\ A^\phi &= \int_h b\phi^{(k)} E_x^{(k)} dz; B^\phi = \int_h bz\phi^{(k)} E_x^{(k)} dz; D^\phi = \int_h b\phi^{2(k)} E_x^{(k)} dz; \\ A_t &= \int_h bG_{xz}^{(k)} dz; B_t = \int_h b\beta^{(k)} G_{xz}^{(k)} dz; D_t = \int_h b\beta^{2(k)} G_{xz}^{(k)} dz \end{aligned} \quad (16)$$

Note that the RZT requires only  $C^0$ -continuity condition on the selection of the shape functions in FE formulation. Thus, as for TBT elements, the simplest RZT-based element is a two-node element with linear Lagrangian shape functions. For further details, the interested readers are addressed to the full FE formulation reported in Ref. Gherlone et al. (2011), Di Sciuva et al. (2015).

### 2.6. Numerical multi-scale analysis

In this Section, the second-order Multi-Scale analysis for the study of beam cross-sections and its homogenization procedure are briefly explained.

Recalling the general description of MS analysis and the micro-macro modelization scheme given in the introductory Section 1, the main objective of this approach is obtaining the 2D constitutive behaviour of the beam's cross-section using a homogenization procedure over its micro-model representation. In a bi-dimensional case, micro-models or RVEs are Plane-Stress (PS) representations of the beam's longitudinal sections in their plane  $xz$ , whereas the macro-models are described as bi-dimensional Timoshenko Beam (TB) models.

The first key aspect to consider in this MS analysis is the scale separation between the micro and macro scales in the beam's axial direction. This separation entails that PS micro-models represent an infinitesimal portion of the total macro-model's length, and therefore, the strain distribution in any point of the macro-scale is seen as almost constant in the micro-models. Otherwise, in the transverse direction  $z$ , the micro-model reproduces the entire thickness length, and therefore, there is no such scale separation. For this reason, if curvature phenomena need to be captured, it will be necessary to take into account the axial variation of the deformation along this direction.

Given the derivative relationship between strain and displacements, the kinematics on the micro-model can be approximated using a low-order Taylor series. Due to the aforementioned hypothesis, it is required to use at least a second-order series to capture the curvature and its linear axial strain variation through the thickness direction. For the 2D case, the displacement field approximation  $\mathbf{u}^\mu = \{u_x^\mu, u_z^\mu\}$  for any point  $\mathbf{X}_\mu = \{X_\mu, Z_\mu\}$  in a PS micro-model representation would be given by

$$\mathbf{u}^\mu = (\mathbf{F}(\mathbf{X}_M) - \mathbf{I}) \cdot \mathbf{X}_\mu + \frac{1}{2} \cdot \mathbf{X}_\mu^T \cdot {}^3\mathbf{G}(\mathbf{X}_M) \cdot \mathbf{X}_\mu + \boldsymbol{\omega}, \quad (17)$$

where  $\mathbf{F}$  and  ${}^3\mathbf{G}$ , are the first and second-order deformation gradients in a point of the macro-model  $\mathbf{X}_M = \{X_M, Z_M\}$  and  $\boldsymbol{\omega} = \{\omega_x, \omega_z\}$  represents the fluctuations of such approximation.

Those two deformation gradients can be derived directly from the kinematics of the macro-model, given a constant state of deformation. In the case of working with a Timoshenko beam model, the centred co-rotational kinematic field  $\mathbf{x}^{\text{TB}} = \{x^{\text{TB}}, z^{\text{TB}}\}$  described in the  $\{x, z\}$  system of reference for a  $\mathbf{X}_M$  point and its spatial vicinity coordinates  $\mathbf{x}_M = (x_M, z_M)$ , is obtained by integrating Eq. (5) assuming that the pure strain components  $u_{,x}$ ,  $\theta_{,x}$  and  $\gamma_{xz}$  remain constant, as

$$\begin{aligned} x_M^{\text{TB}}(\mathbf{X}_M, \mathbf{x}_M) &= x(\mathbf{X}_M) + u_{,x}(\mathbf{X}_M)x_M + \gamma_{xz}(\mathbf{X}_M)z_M + \theta_{,x}(\mathbf{X}_M)z_M x_M \\ z_M^{\text{TB}}(\mathbf{X}_M, \mathbf{x}_M) &= z_M(\mathbf{X}_M) - \frac{\theta_{,x}(\mathbf{X}_M)}{2} x_M^2 \end{aligned} \quad (18)$$

From it,  $\mathbf{F} = \nabla \mathbf{x}^{\text{TB}}$  and  ${}^3\mathbf{G} = \nabla \mathbf{F}$ , being  $\nabla = (\frac{\partial}{\partial x}, \frac{\partial}{\partial z})$ , correspond to

$$\mathbf{F}(\mathbf{X}_M) = \begin{bmatrix} \frac{\partial x^{TB}}{\partial x} & \frac{\partial x^{TB}}{\partial z} \\ \frac{\partial z^{TB}}{\partial x} & \frac{\partial z^{TB}}{\partial z} \end{bmatrix} = \begin{bmatrix} 1 + u_{,x}(\mathbf{X}_M) & \gamma_{xz} \\ 0 & 1 \end{bmatrix} \quad \text{and} \\ {}^3\mathbf{G}(\mathbf{X}_M) = \left\{ \left[ \frac{\partial \mathbf{F}}{\partial x} \right], \left[ \frac{\partial \mathbf{F}}{\partial z} \right] \right\} = \left\{ \begin{bmatrix} 0 & \theta_{,x} \\ -\theta_{,x} & 0 \end{bmatrix}, \begin{bmatrix} \theta_{,x} & 0 \\ 0 & 0 \end{bmatrix} \right\},$$

where,  $\mathbf{F}$  and  $\mathbf{G}$  are evaluated at and only at the  $\mathbf{X}_M$  point. Therefore, only the constant components not related to the spatial vicinity  $\mathbf{x}_M$  of such point are considered. For this reason, within  $\mathbf{F}$  only the axial deformations with a constant distribution are represented, thus omitting  $\theta_{,x}$  components, while the second-order gradient  ${}^3\mathbf{G}$  does reflect the variant deformation associated with the curvature.

The second key aspect to take into account in a Multi-Scale analysis is the fulfilment of the average strain theorem (Otero et al., 2018). As its name suggests, this theorem relates the state of deformation at an infinitesimal point of the macro-model with the average of the deformation in the corresponding RVE. These can be calculated by integrating the deformation over the entire RVE domain and then dividing it by its volume.

Applying the displacement field described in Eq. (17) and satisfy the stated theorem requires the definition of a boundary condition set over the RVE. There exist different sets of boundary conditions that fulfil the requirements, distinguished between them by the degree of fluctuation  $\omega$  allowed in the micro-model. In order to achieve the desired deformation, the combination proposed by Geers et al. at Geers et al. (2007) are used. They consist of imposing a kinematic periodic condition on the axial displacements between the two opposite edges in the axial direction of the micro-model, together with a minimal-periodicity relationship between the tangential displacements with an integral form.

In a discrete model, the former boundaries can be achieved by imposing the axial fluctuation relationship,  ${}^R\omega_x = {}^L\omega_x$ , between all the pairs of nodes aligned in opposite edges, Right and Left. Applying this condition in Eq. (17) leads to the displacement relationship

$${}^R u_x^\mu - {}^L u_x^\mu = (\mathbf{F} - \mathbf{I}) \cdot ({}^R \mathbf{X}_\mu - {}^L \mathbf{X}_\mu) \cdot \{1, 0\}^T + \frac{1}{2} \cdot ({}^R \mathbf{X}_\mu - {}^L \mathbf{X}_\mu)^T \cdot {}^3\mathbf{G} \cdot ({}^R \mathbf{X}_\mu - {}^L \mathbf{X}_\mu) \cdot \{1, 0\}^T \quad (19)$$

where  $\mathbf{F}$  and  $\mathbf{G}$  are constant through the RVE, and therefore shared by the two nodes, and the  ${}^L \mathbf{X}_\mu$  and  ${}^R \mathbf{X}_\mu$  are the position of the opposite left and right nodes respectively.

This periodic boundary condition is expressed in an integral relationship between the Left and Right tangential components of the fluctuation, as follows

$$\int ({}^R \omega_z - {}^L \omega_z) d\Gamma = 0. \quad (20)$$

When the reference system used to define the RVE model is placed in the middle of its longitudinal span, this combination can be expressed in terms of displacements as

$$\int ({}^R u_z^\mu - {}^L u_z^\mu) d\Gamma = 0. \quad (21)$$

The Fig. 4 shows a schematic representation of the resulting kinematics when these boundary conditions are applied for each one of the pure strain states, i.e. when one of the  $u_x$ ,  $\theta_x$  or  $w_x + \theta$  components is different to zero. Note that the grey colour-shape represents the initial geometry of the RVE, and the black line is its final contour. As can be observed, this combination is insufficient to induce the out-of-plane shear deformation since, as represented by the black contour in Fig. 4(c), it exists a resultant kinematic, that is compatible with such periodicity, and it neutralizes the intended deformation by matching the initial shape.

In order to force the desired out-of-plane shear deformation, represented by the red contour line in the same Fig. 4(c), the second above-mentioned condition is introduced in integral form as

$$0 = \int Z_\mu \cdot {}^L \omega_z d^L \Gamma. \quad (22)$$

This constraint avoids inconsistencies in the axial displacement distributions through the enforcement of the vanishing condition of the first moment of fluctuations with respect to the Z-axis. Rewriting Eq. (22) using the micro-scale displacement notation, it yields

$$\int Z_\mu \cdot {}^L \omega_z d^L \Gamma = \int Z_\mu \cdot ((\mathbf{F} - \mathbf{I}) \cdot \mathbf{X}_\mu + \frac{1}{2} \cdot \mathbf{X}_\mu^T \cdot {}^3\mathbf{G} \cdot \mathbf{X}_\mu) \cdot \{0, 1\}^T d^L \Gamma. \quad (23)$$

It should be noted that with the described BCs, the average value theorem is fulfilled for the  $u_x$  and  $\omega_x + \theta$  components; however, in the other directions, it may not, for instance, the case of a micro-model under longitudinal tension undergoing compressing deformation in the out-of-plane direction due to Poisson's effect. However, following the kinematics of the Timoshenko beam model (see, Eq. (4)), these quantities should not exist, and therefore, their average values should be zero. This inconsistency is explained by the simplifications introduced in the beam model, where the transverse normal stresses, with respect to the beam axis, are assumed to be negligible and, therefore, so are their deformations. For this reason, the strains in that direction cannot be compared with the ones represented in the full bi-dimensional model as the ones found in the micro-scale. Since they are not considered in the beam macro-model, they are simply indeterminate.

Once the relationship between macro-level deformation and micro-scale kinematics has been defined, the further step is considering the homogenization procedure to characterize the RVEs at a constitutive level. In a linear analysis, this homogenization procedure takes place at the beginning of the simulation, and the involved steps are the following ones.

Firstly, a plane-stress RVE that accurately represents the beam section and its lamination scheme is modelled using two-dimensional finite elements based on higher-order shape functions (required to avoid the shear-locking phenomena associated with bi-dimensional linear elements).

Then, the mechanics of this RVE are simulated by enforcing the periodic boundary conditions and independently evaluating each deformation state, e.g., membrane uniform, pure bending, and pure shear.

From these preliminary analyses, the induced stresses in the RVE are averaged following the Hill-Mandel principle (Otero et al., 2018). This principle establishes a direct relationship between the virtual work done at any point of the macro-model and the average of the stresses of the RVE that represents it. If the latter is defined by a domain  $\Omega$  and with a length  $L$ , its averaged integrated stresses are given by

$$N_o = \frac{1}{L} \int \sigma_{xx} d\Omega, \quad M_o = \frac{1}{L} \int Z_\mu \sigma_{xx} d\Omega, \quad T_o = \frac{1}{L} \int \tau_{xz} d\Omega. \quad (24)$$

It is worth noting that no correction factor is required for the shear component.

The resulting constitutive relationships between each pure strain state and the induced averaged stresses are re-arranged in the form of a constitutive tensor, as the one shown in Eq. (7), and also adopted in the definition of the macro-model stiffness matrix.

## 2.7. Mixed dimensional coupling

In this section, the fundamentals of the work-based Mixing Dimensional Coupling (MDC) and its application to the definition of 2D Beam-Like Reduced Order Models are explained (BLROM) (Turon et al., 2024).

The MDC is a technique introduced by McCune et al. (2000) that aims to couple models with different kinematic and/or dimensions. In order to perform these couplings, the fundamentals of MDC rely on the equilibrium of energy in the form of work done on the contact area between the interfaced models. Assuming that the models are in contact but must not overlap, these areas can be seen as an interface surface that has two sides, each one belonging to a different model. A schematic representation of this concept is shown in Fig. 5 where

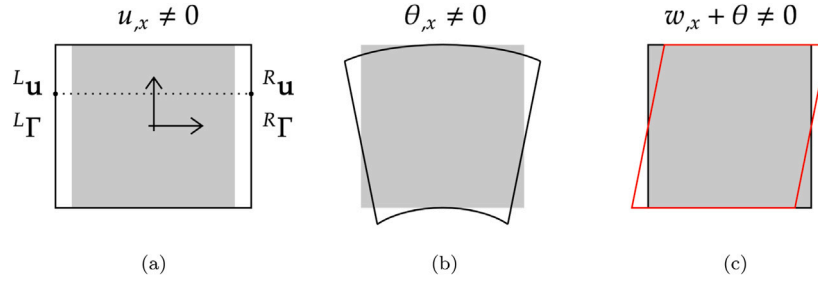


Fig. 4. Homogenization strain states applying Periodic BC on the RVE.

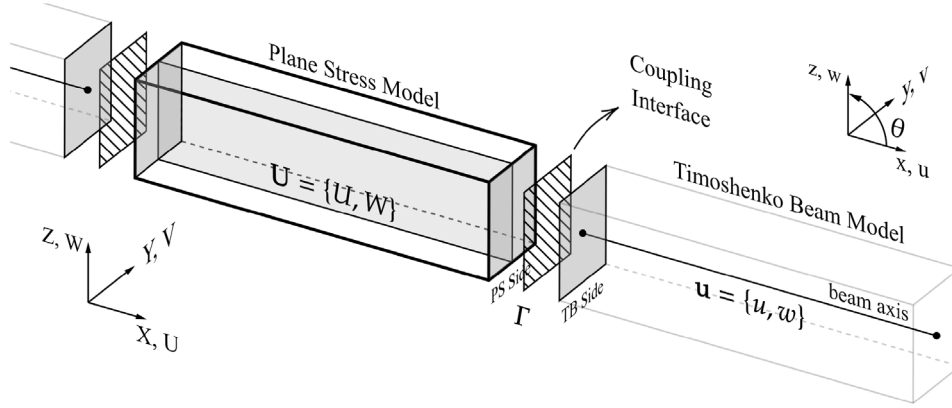


Fig. 5. Schematic representation of two models coupled with the MDC.

a Timoshenko Beam (TB) model is being coupled with its analogous Plane-Stress (PS) model. If the normal direction of a side is aligned with the first axis of the reference system, the work on it is quantified as the product between the traction force vector, i.e.  $\mathbf{t}$ , in the side and its displacements such that

$$\mathbb{W}_{2D} = \int_A \mathbf{t} \cdot \mathbf{u} \, dA \quad (25)$$

where, in a bi-dimensional case described on the  $XZ$  plane and using a system of reference perpendicular to the interface,  $\mathbf{t} = \boldsymbol{\sigma} \cdot \mathbf{n} = \{\sigma_{xx}, \tau_{xz}\}$ , with  $\mathbf{n} = \{1, 0\}$ , and  $\mathbf{u} = \{u_x, u_z\}$ .

Therefore, following with the example depicted in Fig. 5, the equilibrium of work,  $\mathbb{W}$ , and reactions,  $\mathbf{P} = \{N, M, T\}$ , on the interface is given by

$$\mathbb{W}_\Gamma^{\text{PS}} = \int_{\Gamma^{\text{PS}}} \boldsymbol{\sigma}^{\text{PS}} \cdot \mathbf{U} \, d\Gamma = \int_{\Gamma^{\text{TB}}} \boldsymbol{\sigma}^{\text{TB}} \cdot \mathbf{u} \, d\Gamma = \mathbb{W}_\Gamma^{\text{TB}} \quad (26)$$

and

$$\mathbf{P}^{\text{PS}} = \mathbf{P}^{\text{TB}} \quad (27)$$

where  $\boldsymbol{\sigma}^{\text{PS}}$  and  $\boldsymbol{\sigma}^{\text{TB}}$  are the axial stress distribution from each model,  $\Gamma^{\text{PS}}$  and  $\Gamma^{\text{TB}}$  are the domains of each side of interface respectively and  $\mathbf{U}$  and  $\mathbf{u}$  are the displacement fields for the PS and TB models.

The stress distributions in each domain are obtained analytically for a given load  $N$ ,  $M$  or  $T$ , and considering a PS and a TB kinematics, they correspond to

$$\sigma_{xx}^{\text{PS}}(z) = \sigma_{xx}^{\text{TB}}(z) = \{N \quad M\} \cdot \mathbb{D}_I^{-T} \cdot \begin{Bmatrix} E_x(z) \\ E_x(z)z \end{Bmatrix} = \{N \quad M\} \cdot I_U \quad (28)$$

and

$$\tau_{xz}^{\text{TB}}(z) = T \cdot \mathbb{D}_S^{-1} \cdot G_{xz}(z), \quad (29)$$

$$\tau_{xz}^{\text{PS}}(z) = \{T \quad 0\} \cdot \left[ \int_h^z d_A dz \quad \int_h^z d_B dz \right]^{-T} \cdot \begin{Bmatrix} d_A \\ d_B \end{Bmatrix} = \{T\} \cdot I_W \quad (30)$$

with

$$\begin{aligned} d_A(z) &= \int_{h^-}^z b E_x^{(k)} dz \\ d_B(z) &= \int_{h^-}^z b z E_x^{(k)} dz \end{aligned} \quad (31)$$

Working with the analytical stress distribution makes it unnecessary to apply any correction factor associated with shear deformation.

Replacing such distributions to Eq. (26) together with the displacement fields  $\mathbf{U}$  and  $\mathbf{u}$ , from each side of the interface, leads to

$$\{N \quad M\} \cdot \int_{\Gamma^{\text{PS}}} I_U \cdot U \, d\Gamma + \{T\} \cdot \int_{\Gamma^{\text{TB}}} I_W \cdot W \, d\Gamma = \mathbf{P} \cdot \mathbf{u}^{\text{TB}} \quad (32)$$

where, on the right-hand side, the TBT kinematic variables  $\mathbf{u}^{\text{TB}} = \{u, \theta, w\}$  and the original definition of  $N$ ,  $M$  and  $T$  are used to simplify the integration over  $\Gamma^{\text{TB}}$ . Applying Eq. (27) and performing further simplifications Eq. (32) becomes

$$\mathbf{P} \cdot (\mathbf{c}_U(\mathbf{U}) - \mathbf{u}^{\text{TB}}) = 0. \quad (33)$$

The expression in Eq. (33) follows the same mathematical form as a Lagrange Multiplier (LM) condition,  $\lambda g(x) = 0$ , being  $\mathbf{P}$  the Lagrange multiplier itself. The coefficients arising within the integrals of the PS side of the coupling condition  $\mathbf{c}_U$  are applied over the nodal degrees of freedom of the interface and will depend on the lamination of the beam and the properties of each layer.

This technique can be used to define BLROM compatible with beam elements. Nevertheless, instead of coupling two models, this approach requires isolating the PS representation of a beam with two interfaces, one in each end (Left and Right) as shown in Fig. 5, then the coupling of each interface are used for defining the DOFs corresponding to the BLROM itself. The energy  $L$  related to this system would be composed by

$$L(\mathbf{U}, \mathbf{u}^{\text{TB}}, {}^L\mathbf{P}, {}^R\mathbf{P}) = \Pi_{\Omega}^{\text{PS}}(\mathbf{U}) + \quad (34)$$

$${}^L\mathbf{P} \cdot ({}^L\mathbf{c}_U(\mathbf{U}) - {}^L\mathbf{u}^{\text{TB}}) + {}^R\mathbf{P} \cdot ({}^R\mathbf{c}_U(\mathbf{U}) - {}^R\mathbf{u}^{\text{TB}}), \quad (35)$$

where  $\Pi_{\Omega}^{\text{PS}}$  is the inner energy associated with the PS model, and the extra terms are the coupling conditions of each one of the interfaces in the LM condition form.



**Table 1**  
Materials and corresponding mechanical properties, elastic and shear moduli are given in GPa.

Mat. ID	$E_1$	$E_2$	$E_3$	$\nu_{12}$	$\nu_{13}$	$\nu_{23}$	$G_{12}$	$G_{13}$	$G_{23}$
A	300	12	12	0.25	0.25	0.25	6	6	2.4
B	131	10.34	10.34	0.22	0.22	0.49	1	6.205	1
C	0.0403	0.0403	0.0403	0.3	0.3	0.3	0.012	0.012	0.012
D	73	73	73	0.33	0.33	0.33	27.444	27.444	27.444

**Table 2**  
Beam nomenclature and laminate stacking sequence (from bottom to top layer).

ID	Materials	Orientation [deg]	Normalized thickness ( $h^{(k)}/h$ )
B1	A/A/A/A/A/A	0/90/0/90/0/90/0	$\frac{1}{7}/\frac{1}{7}/\frac{1}{7}/\frac{1}{7}/\frac{1}{7}/\frac{1}{7}$
B2	A/A/C/A/A	0/90/0/90/0	0.125/0.125/0.5/0.125/0.125
B3	A/B/B/C/D/C/B/A	0/0/90/0/0/0/90/0	0.05/0.1/0.05/0.2/0.1/0.3/0.15/0.05

Minimizing this energy form by deriving it with respect to the involved variables yields the following linear system (written for convenience in a useful matrix notation)

$$\begin{bmatrix} \mathbf{K}_{LL} & \mathbf{K}_{Li} & \mathbf{K}_{LR} & \mathbf{L}\mathbf{c}_U^T & 0 \\ \mathbf{K}_{iL} & \mathbf{K}_{ii} & \mathbf{K}_{iR} & 0 & 0 \\ \mathbf{K}_{RL} & \mathbf{K}_{Ri} & \mathbf{K}_{RR} & 0 & \mathbf{R}\mathbf{c}_U^T \\ \mathbf{L}\mathbf{c}_U & 0 & 0 & 0 & 0 \\ 0 & 0 & \mathbf{R}\mathbf{c}_U & 0 & 0 \end{bmatrix} \cdot \begin{bmatrix} \mathbf{U}_L \\ \mathbf{U}_i \\ \mathbf{U}_R \\ \mathbf{L}\mathbf{P} \\ \mathbf{R}\mathbf{P} \end{bmatrix} = \begin{bmatrix} 0 \\ 0 \\ 0 \\ \mathbf{L}\mathbf{u}^{\text{TB}} \\ \mathbf{R}\mathbf{u}^{\text{TB}} \end{bmatrix} \quad (36)$$

being  $\mathbf{K}$  the stiffness matrix of the PS model at the internal nodes  $i$ , the nodes belonging to the Left interface and the nodes belonging to the Right interface.

Finally, through a static condensation procedure, the DOFs represented by  $\mathbf{U}$  associated with the PS model are reduced, only leaving the relationship between  $\mathbf{u}^{\text{TB}}$  and  $\mathbf{P}$ , equivalently to the stiffness matrix of the BLROM. A more detailed description of this same procedure can be found in the referenced article (Turon et al., 2024).

### 3. Numerical analysis

This section undertakes a comprehensive numerical investigation to evaluate the primary advantages and drawbacks of each numerical model, specifically for multilayered composite and sandwich beams in cylindrical bending conditions. In this numerical assessment, two configurations are addressed considering different loading cases and Boundary Conditions (BCs) which are typical of engineering applications. The first one consists of a Clamped Edge (CE) beam with an imposed transverse displacement on its free end; the second one reproduces a typical Three-Point Bending test (3PB), with a prescribed displacement at the beam mid-span. In addition, for each configuration multiple lamination schemes are considered. The material mechanical properties and laminate stacking sequences for each beam case (from bottom to top layer) are listed in Table 1 and 2, respectively.

Note that for the TBT elements, as previously detailed, appropriate shear correction factors computed using Raman-Davlos/Oñate (Madabhushi-Raman and Davalos, 1996; Oñate, 2013) methods are adopted: for beam B1,  $k_f = 0.6757$ ; for beam B2,  $k_f = 0.008682$ ; for beam B3,  $k_f = 0.004834$ .

No shear correction factors are required for the other models. The numerical results obtained with approximated FE models are compared with their corresponding high-fidelity FE models using MSC-Patran/Nastran codes. Each beam configuration is discretized with 2D-SOLID QUAD8 NASTRAN elements with the Plane-Stress option. Moreover, Table 3 summarizes the NASTRAN model discretizations for each beam lamination and load/BC configuration.

The discretization adopted for TBT and RZT FE models is the same for each beam lamination scheme and load configuration. Table 4 summarizes the FE model characteristics in terms of number of elements, nodes and DOFs present in the beam models. As reported in Table 4, the large amount of finite elements used to represent the multilayered

composite and sandwich beams in this study has been selected to: guarantee the convergence of the FE solution; obtain a highly-refined approximation of strain and stress distributions in each element; avoid any occurrence of shear-locking problems that affect coarse discretizations using low-order finite elements, such as TBT/RZT-based elements. Although different methodologies for managing this issue can be applied, this numerical analysis does not cover slender beam cases; thus, full integration schemes and high-refined meshes are considered for each element type. The interested reader may find more details on the convergence behaviour of RZT/TBT-based elements in Refs. Gherlone et al. (2011), Oñate et al. (2012), Oñate (2013). Additionally, even though the number of beam elements for TBT/RZT and MS models seems high, the computational cost (in terms of total DOFs) required for the static analysis is less than that necessary for the high-fidelity models. Moreover, the adopted numerical models and their corresponding elements are developed in the framework of linear elasticity; thus, the small-scale effect that might affect the solution in the  $x$  direction using the selected discretizations does not affect the validity of the models when compared with the high-fidelity FE solution.

In the homogenization procedure for MS FE mode, a PS micro-model is defined for each lamination scheme. Each micro-model has a length of 0.1 mm, and their heights correspond to the laminate thickness, i.e. 1 mm. The discretization is performed with the same elements used in the high-fidelity model and with an equivalent average element edge length, i.e. 0.01 mm. This choice guarantees a considerably high number of elements for each layer in the thickness direction.

During the homogenization procedure, a constitutive relationship is obtained for each laminate. These are in agreement with the constitutive relationship computed with Eq. (7) and (9). Only a small deviation ( $\approx 10\%$ ) in the  $\mathbb{D}_S$  component could be observed. This deviation depends on the lamination scheme and rises with the value of the ratio  $\mathbb{D}_I/\mathbb{D}_S$ . Moreover, as earlier detailed in the model formulation, no shear corrector factor is required. Thus, the macro-model adopted in the MS analysis has the same characteristics as the TBT, with the care of using the constitutive relationships coming from the homogenization procedure.

Finally, the PS 2D models used to define the BLROM elements have a micro-scale length of 0.5 mm, and their height corresponds to the height of the laminates, as for the previous case. The discretization of these models is also performed with the same elements used for the high-fidelity model. However, these have an average edge length of 0.02 mm. Nevertheless, it is guaranteed that all layers represented have a minimum of 3 elements in their thickness direction.

For instance, Fig. 6 shows the model corresponding to laminate B3 subjected to each of the degrees of freedom present in the equivalent BLROM analysed during the condensation procedure.

As the BLROMs are obtained by reducing a 0.5 mm model, each element will represent an equivalent length when assembled.

**Table 3**  
High-fidelity NASTRAN model characteristics: number of elements, nodes and DOFs.

Beam ID	CE			3PB		
	$N_{el}$	$N_{nodes}$	DOFs	$N_{el}$	$N_{nodes}$	DOFs
B1	$600 \times 98$	177 797	355 594	$1200 \times 49$	178 899	357 798
B2	$600 \times 102$	185 005	370 010	-	-	-
B3	$600 \times 100$	181 401	362 802	$1200 \times 50$	182 501	365 002

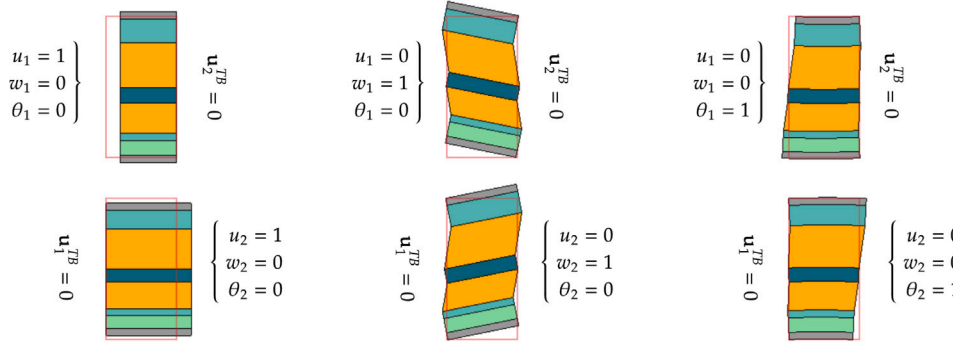


**Fig. 6.** Condensation procedure for laminate B3.

**Table 4**  
Beam FE model characteristics: number of elements, nodes and DOFs.

MODEL	$N_{el}$	$N_{nodes}$	DOFs
TBT	1000	1001	3003
RZT	1000	1001	4004
MS (macro-model)	1000	1001	3003
BLROM	12	13	39

**Table 5**  
BCs at each beam edge: kinematic variable constraints and values (in mm).

	$x = 0$	$x = L$
NASTRAN	$u = 0, w = 0$	$w = -1$
TBT	$u = 0, w = 0, \theta = 0$	$w = -1$
RZT	$u = 0, w = 0, \theta = 0, \psi = 0$	$w = -1$
MS	$u = 0, w = 0, \theta = 0$	$w = -1$
BLROM	$u = 0, w = 0, \theta = 0$	$w = -1$

### 3.1. Clamped edge (CE)

In this study, a clamped beam of length  $L = 6$  mm is subjected to bending analysis. The BCs are specified accordingly: fully clamped left edge, i.e. no displacements and no rotation are allowed; free right edge with a prescribed transverse displacement (p.d.) of  $-1$  mm across the whole laminate thickness. Table 5 resumes the constraints in terms of kinematic variables applied to each investigated model, and Fig. 7 schematically represents the beam's geometry and its BCs.

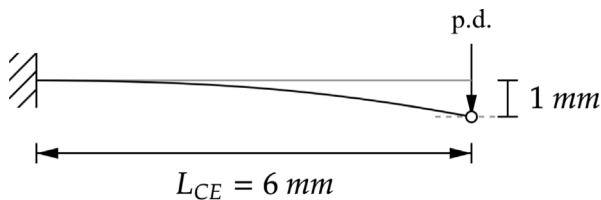


**Fig. 7.** CE beam configuration: geometry and BCs.

The results obtained are presented hereafter.

#### 3.1.1. Transverse deflection

The transverse beam deflections along the axis are here compared with the reference solutions ( $\bar{w}(x)$ ) provided by the NASTRAN 2D models. Since the FE beam models, i.e. TBT/RZT, do not include the transverse normal deformability, the reference transverse displacements are averaged as follows:

$$\bar{w}(x) = \frac{1}{h} \int_h u_z(x, z) dz \quad (37)$$

Figs. 8(a), 8(b), and 8(c) report the transverse displacement for each beam lamination. The RZT elements are able to follow the transverse deformation, especially for the symmetric sandwich beam B2. Conversely, the TBT elements are quite inaccurate in capturing the beam curvature, especially near the clamped edge. In fact, for B2 and B3 beams, the TBT leads to a worse prediction of the transverse displacement along the beam axis.

The MS macro-model reports an almost identical behaviour with respect to the TBT one for each laminate. The reason behind this behaviour is the slight numerical deviation that could be observed in the  $\mathbb{D}_S$  components, which have little impact on the macro-models results.

Despite consisting of significantly fewer elements, the beam models assembled with the BLROM elements behave identically to the TBT models in each one of the analysed laminates.

#### 3.1.2. Through-the-thickness distributions

In this paragraph, the through-the-thickness distributions of axial strain and transverse shear stress are reported. For simplicity, both distributions are evaluated at the beam points corresponding to  $x = 3.0$  mm and  $x = 0.1$  mm, for each lamination scheme.

The four investigated FE models report accurate results for the axial strain distributions in beam B1 closer to the beam mid-span, as can be seen in Fig. 9(a). Conversely, Figs. 9(b) and 9(c) show that the RZT model is generally able to reproduce the typical zigzag behaviour of the strains, especially for B2 and B3 sandwich beams. Clearly, some discrepancies are due to the inability of the RZT formulation to capture the transverse normal deformability, which becomes relevant for lower length-to-thickness ratios. Although the other FE models are not able to capture strain's slope variation across layer interfaces, they are able to provide an approximated value averaged over the thickness.

Figs. 10(a), 10(b), and 10(c) report the through-the-thickness distributions of the transverse shear stress computed using the constitutive

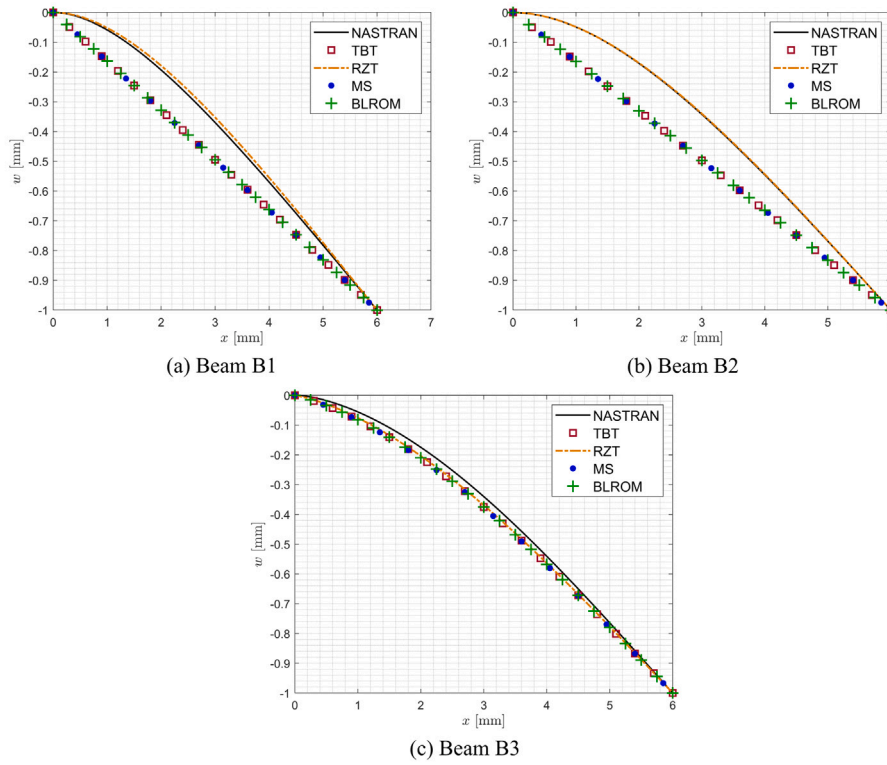


Fig. 8. Transverse deflection (given in mm) for CE load configuration.

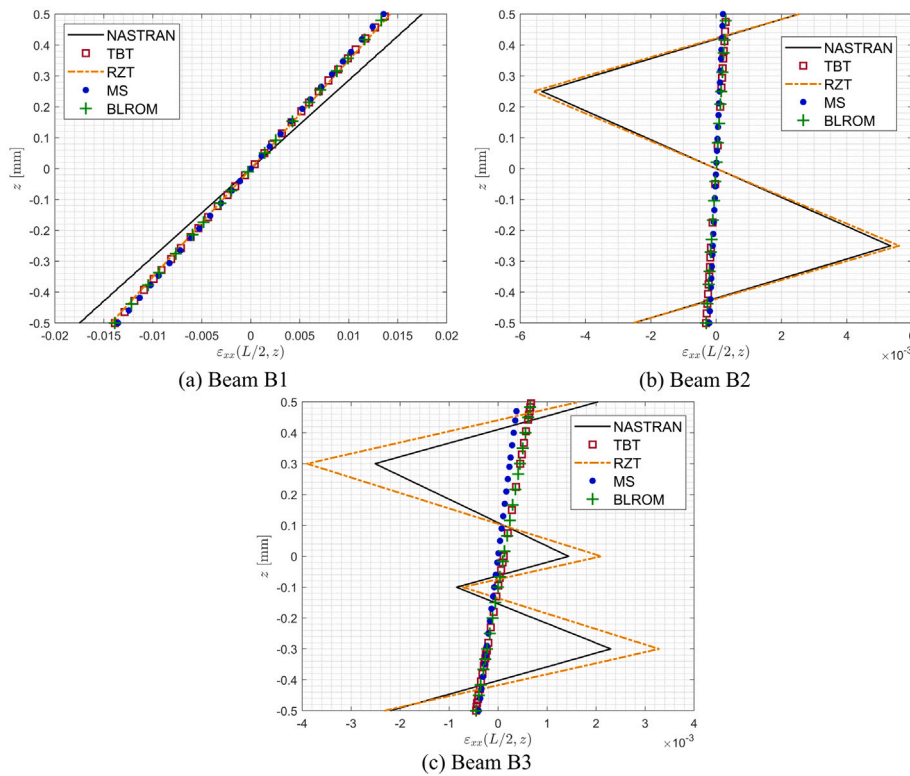


Fig. 9. Axial strain distributions closer to the beam mid-span, i.e.  $x = L/2$ .

material relations, i.e. Eqs. (6). Note that, for the TBT elements, the correction factor has been considered in the constitutive relations. In addition, for the BLROM and MS models, the respective elemental

models and micro-models at the corresponding location are analysed. For instance, Fig. 13 represents the elemental model from B1 BLROM beam located between  $x = 2.5$  and  $x = 3.0$  mm. Each left and right edge

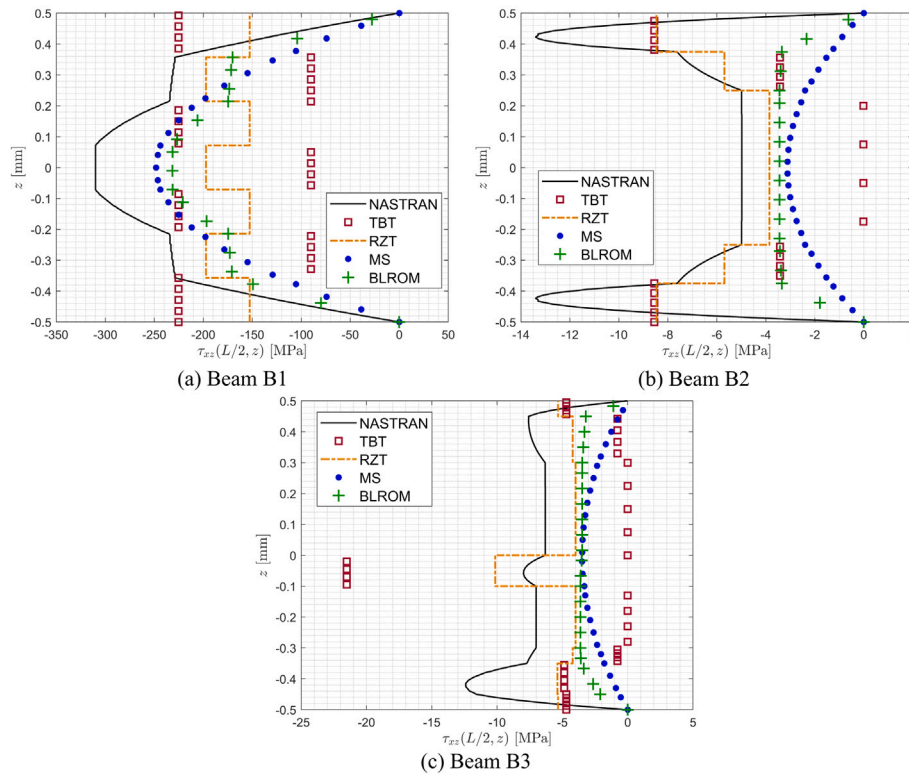


Fig. 10. Transverse shear stress distribution at the beam's mid-span ( $x = L/2$ ).

belongs to an interface that has been loaded with the corresponding nodal DOF values.

Clearly, the TBT and RZT elements cannot reproduce the parabolic piece-wise continuous distribution of the transverse shear stress of the reference solution. In fact, according to the TBT and RZT kinematics and the constitutive material relations, the transverse shear stress distributions are expected to remain constant in each layer with jumps at the interfaces. However, the RZT constant value given in each layer could represent, in an average way, the correct transverse shear deformability for each beam case. Conversely, the TBT model demonstrates greater inaccuracy in transverse stress predictions, particularly in the middle layers of beams B2 and B3, even when a shear correction factor is applied to enhance the model's shear deformability. For TBT and RZT models, a parabolic piecewise distribution can be obtained using the *a-posteriori* stress recovery technique, i.e. integrating the axial stress in Cauchy's equation. However, as detailed earlier, this approach cannot be implemented in low-order finite elements considered in this study. The BLROM model is able to approximate a realistic parabolic piece-wise continuous distribution of the stresses in the B1 beam. This is not the case for beams B2 and B3 where, as shown in Fig. 8, the BLROM model does not capture the beams's deflection and curvature kinematics. The MS model shows a continuous and parabolic stress distribution across the thickness caused by the deformations induced in the micro-models.

The strains near the clamped edge are reported in Figs. 11(a)–11(c). By comparing the results obtained at the beam mid-span, see Fig. 9, higher strains are observed here and, due to the clamped boundary condition, additional zig-zag shaped strains, not present in the middle of the beam appear, as it can be seen in B1 beam. The RZT is the only model able to reproduce the zigzag behaviour of the strains in all beams; meanwhile, the TBT, MS and BLROM models are blind to the boundary effects and are only capable of providing an average result.

Figs. 12(a), 12(b), and 12(c) show the transverse shear stresses distribution near the clamped edge. The shape of stress distributions obtained with the TBT, MS and BLROM models match the stress shapes

Table 6

Boundary conditions at each beam edge: kinematic variable constraints (displacements are given in mm).

	$x = L/4 = L3/4$	$x = L/2$
NASTRAN	$w = 0$ at $z_B$	$u = 0$ and $w = -1$ at $z_T$
TBT	$w = 0$	$u = 0, w = -1$
RZT	$w = 0$	$u = 0, w = -1$
MS	$w = 0$	$u = 0, w = -1$
BLROM	$u = 0$	$u = 0, w = -1$

induced in the middle of the beam, but with a different amplitude, supporting once again the fact that these models are not able to take into account this type of clamping boundary condition. Conversely, the RZT is capable of predicting a change in the transverse shear profile along the beam axis, as can be seen by comparing the results obtained in the middle of the beam and near the clamped edge.

### 3.2. Three-point bending (3PB) problem

The following study aims to simulate a three-point bending test. In light of the results obtained in the previous example, the purpose of these studies is to assess the behaviour of the bending rotation when no restrictions are enforced. In fact, the BCs here considered are located at  $x = 0.25L$ ,  $x = 0.5L$  and  $x = 0.75L$ , where the total length of the beam  $L$  is 24 mm. The two side restrictions prevent transverse displacement, while the central constraint blocks displacement in  $x$  and has a prescribed transverse displacement of  $-1$  mm. Table 6 summarizes the constraints in terms of kinematic variables applied to each model, and Fig. 14 represents the beam's geometry and its BCs.

In view of the earlier results for CE beam configuration, this study is limited only to beams B1 and B3 since sandwich B2 could be seen as a simplified case of B3 configuration.

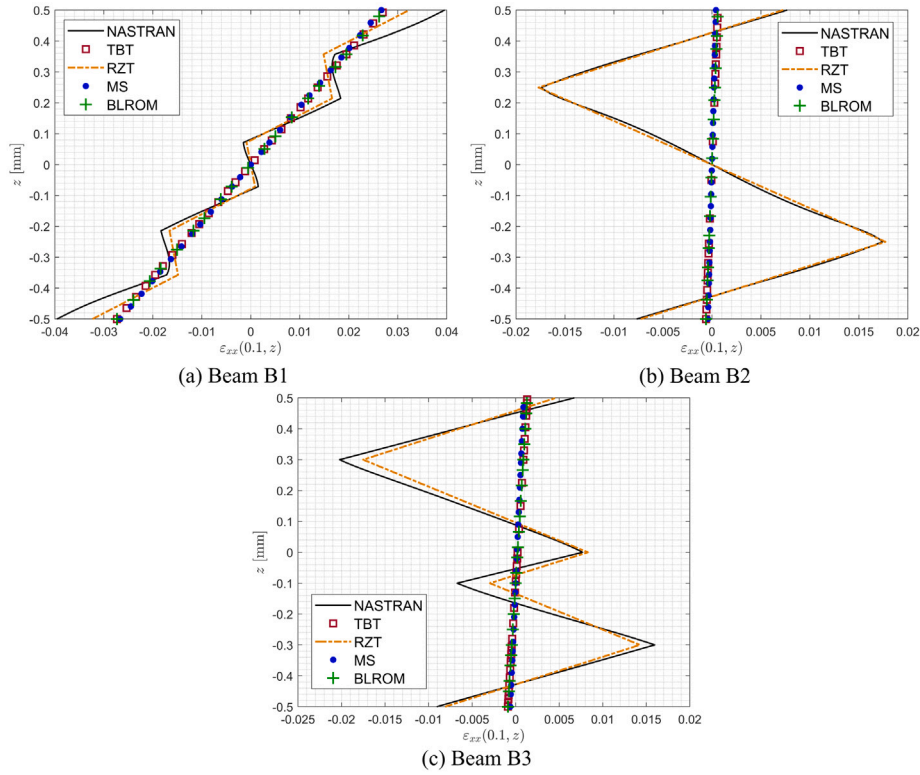


Fig. 11. Through-the-thickness axial strain distributions near the clamped edge ( $x = 0.1$  mm).

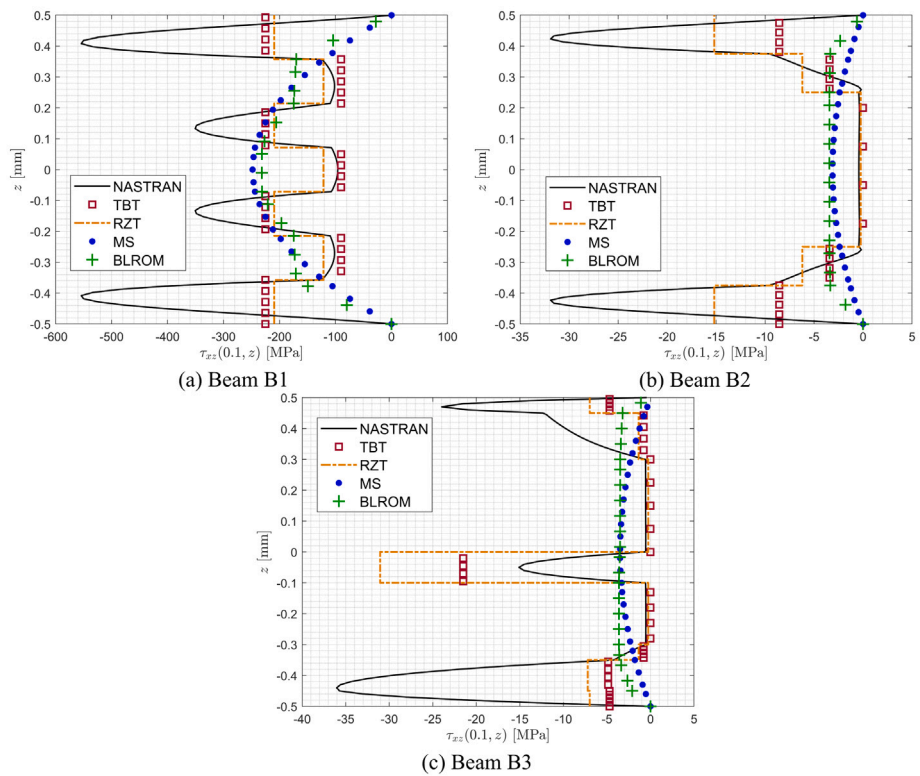


Fig. 12. Through-the-thickness transverse shear stress distributions near the clamped edge ( $x = 0.1$  mm).

### 3.2.1. Transverse deflection

The transverse deflections along the beam axis obtained using the approximated FE models are compared with the reference solution

provided by the NASTRAN 2D model. Since the reference solution includes the transverse normal deformability, an averaged integral value has been computed using Eq. (37) to effectively compare the

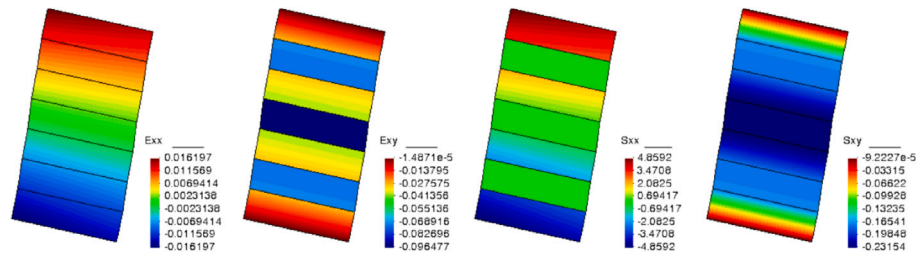


Fig. 13. Strain and stress states of the elemental B1 model located between  $x = 2.5$  mm to  $3.0$  mm.

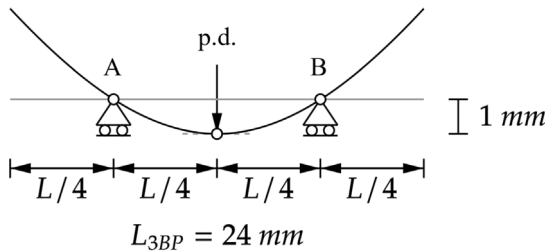


Fig. 14. 3PB beam configuration: geometry and BCs.

displacements with the approximated FE models.

The results for transversal displacements in each model are reported in Figures 15(a) and 15(b), for beam B1 and B3, respectively. Fig. 15(a) shows that for beam B1, the transverse deflection is accurately approximated by all FE models. However, in Fig. 15(b), only the RZT model is able to capture the kinematics of the laminated beam B3. In fact, the results provided by the FE RZT model are in good agreement with those computed using the high-fidelity NASTRAN 2D model. Thanks to the presence of zigzag rotation in the transverse shear strain distribution, the shear deformability is better predicted in both laminate configurations. The structural response of the other FE models for each lamination scheme is nearly identical. For instance, in beam B1, the TBT, MS and BLROM models effectively capture the deflection along the entire beam length, similar to the RZT model. In this laminate configuration, the effect of shear deformability predicted by the RZT model is quite similar to those computed with the other models, even without using any shear correction factors. However, in the B3 beam, the TBT, MS and BLROM models reproduce the same erratic behaviour captured in the B2 and B3 beams of the previous analysis (see Figs. 8(b) and 8(c)). The different sections between the beam's supports do not seem to bend, as the RZT model does in virtue of the effect of the zigzag rotation. In addition, the deflection at the free ends is much lower than that seen in the high-fidelity model.

### 3.2.2. Through-the-thickness distributions

The through-the-thickness distributions of axial strain and transverse shear stress at the point  $x = 3.0$  mm for beams B1 and B3, are shown in Fig. 16. This point is located at the middle of the left part of the free beam span, i.e. between the beam's edge and the support A (see, Fig. 14) at 0.25 of the total beam's length. As shown in Fig. 16, none of the TBT, MS or BLROM models is able to capture the through-the-thickness deformations at this point, which, although small, are not zero. Conversely, the RZT model reflects with a good level of accuracy the through-the-thickness axial strains, reproducing the already-stated zigzag distribution. As seen in the previous case, the RZT model provides an approximation of shearing stresses in which the changes in shear stiffness from layer to layer are appreciated.

Fig. 17 reports the through-the-thickness axial and shear strain distributions for B1 and B3 laminates at the beam position  $x = 9.0$  mm, i.e. located between the support A and the central point where the prescribed transverse displacement is imposed. In this location, for

laminate B1, the through-the-thickness axial strain distributions are very similar among the considered models, and few differences are noticeable, similarly to that observed for the transverse deflection (see Fig. 15(a)). As expected, the predicted transverse shear distributions depend on the model choice; however, in this particular lamination scheme, i.e. B1, the shear deformability is generally well predicted in an average sense from all the models. In fact, this behaviour is further confirmed by the RZT transverse stress distribution for beam B1, see 17(c), which is quite similar to those predicted by the Timoshenko beam model with the inclusion of the shear correction factor. As observed in Fig. 10(a), the BLROM model is the only one able to capture the parabolic piecewise distribution of the transverse shear stress by leading to a very close approximation with respect to the high-fidelity FE solution. The MS model reports a parabolic shear stress distribution, which is in good agreement (in an average sense) with the reference and the BLROM results. For the B3 lamination case, the results clearly demonstrate that the RZT model is the only one capable of accurately reproducing the axial strain distribution. In fact, as reported in Fig. 17(b), the RZT distribution is quite close to the NASTRAN one. Regarding the shear stress distribution shown in Fig. 17(d), the RZT model over-predicts the maximum stress value of the middle layer. However, the average value computed over the entire section is consistent with the same computed using the high-fidelity model. The approximation reached by the TBT, MS and BLROM models is not able to reach the same level of accuracy introduced by the RZT for beam B3, where the zigzag effect is very pronounced. Moreover, the piecewise continuous through-the-thickness distribution of the transverse shear stress predicted by the BLROM model is not sufficiently accurate with respect to the NASTRAN one to estimate correctly the structural behaviour for this laminate configuration.

## 4. Conclusions

In this paper, a novel and critical overview of some advanced Finite Element (FE) approaches for the 2D static analysis of multilayered composites and sandwich beams has been presented. Firstly, a general overview of the properties of some models currently adopted in FE codes has been shown. Specifically, the Timoshenko Beam Theory (TBT) and the Refined Zigzag Theory (RZT) have been recalled for the cylindrical bending analysis, and the beam constitutive relations are presented via the PVDs. Secondly, the Multi-Scale (MS) approach and the Beam-Like Reduced Order Model (BLROM) have been presented in detail for the 2D static analysis of multilayered composite and sandwich beams. As highlighted in the model's description and confirmed by the newly provided results, the TBT-based beam elements require the computation of an appropriate shear correction factor to estimate the transverse shear deformability correctly. Although it could be beneficial to improve the model accuracy for multilayered composite beams, the TBT fails in predicting transverse displacements, strain and stress distributions for sandwich laminate configurations.

The RZT, thanks to its formulation, is able to compute accurate results for both global and local through-the-thickness quantities (i.e. axial strains and transverse shear stresses in an average sense) without requiring any shear correction factor and an affordable computational

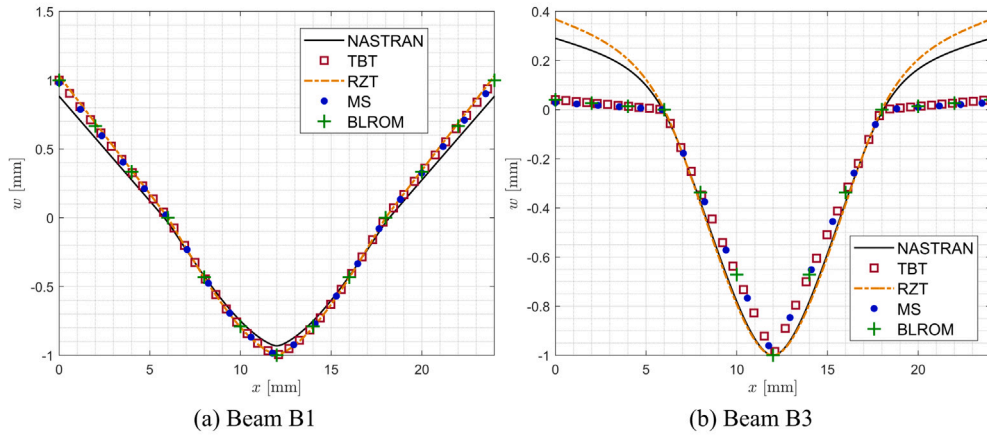


Fig. 15. Transverse deflection (in mm) for 3PB beam configuration.

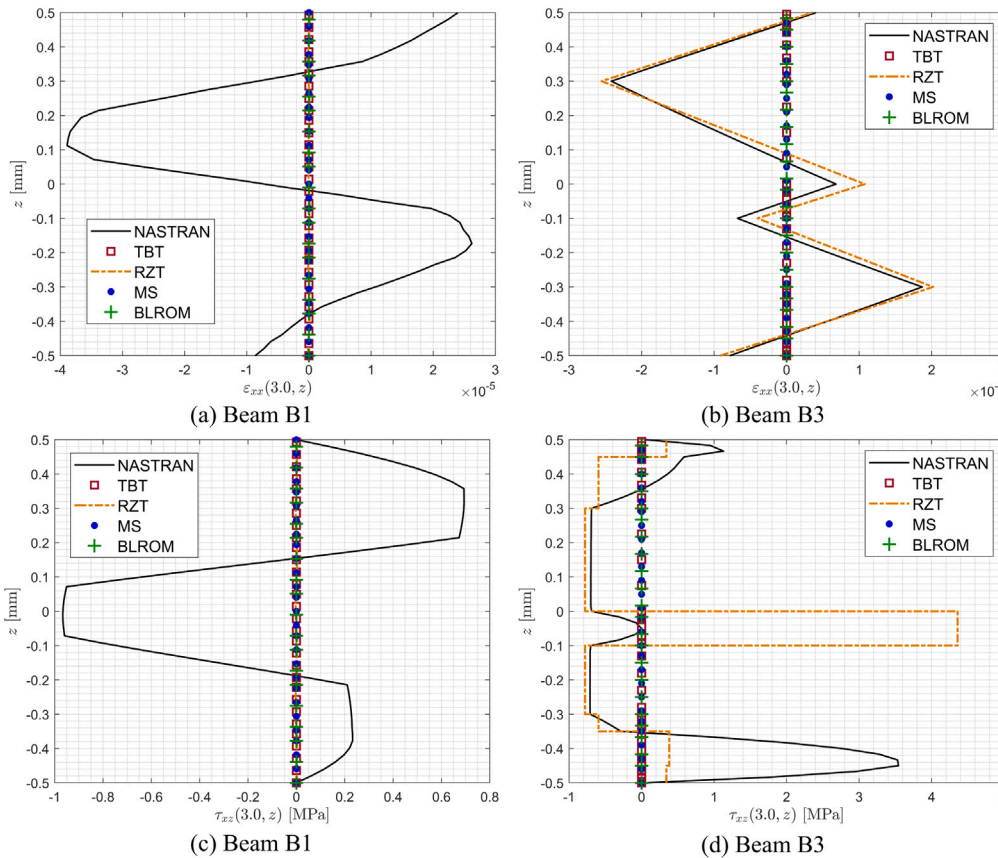


Fig. 16. Through-the-thickness axial strain and shear stress distributions in  $x = 3$  mm.

cost, with respect to the reference high-fidelity solution, as shown in the numerical assessment. Furthermore, remarkable results with the RZT are obtained for highly heterogeneous beams, such as multilayered sandwiches, where the mechanical properties vary a lot across the laminate thickness. However, as expected, the low-order RZT-based elements are not able to reproduce a-posteriori, the typical continuous distributions of the transverse shear stress.

The alternative offered by the MS model, based on the Timoshenko kinematics, provides an equivalent model to the classical TBT for the analysis of multilayered beam and sandwich structures in cylindrical bending conditions, such as those considered in this study. As remarked by the model formulation, one of the most advantageous aspects of

this approach lies in its capability to characterize both simple and heterogeneous lamination schemes at the material constitutive level, including complex geometrical patterns (e.g. honeycomb, lattice structures). A further advantage of the MS model is represented by the homogenization procedure that is able to characterize the TBT constitutive relations without computing any shear correction factor. However, for thick and heterogeneous laminated beams, the MS model fails to reproduce the thickness-wise transverse shear stress distribution. In fact, as shown by the numerical results, the MS formulation can only reproduce continuous parabolic stress functions for each load and BCs configurations, regardless of the beam lamination scheme, which plays an important role for moderately thick beams.

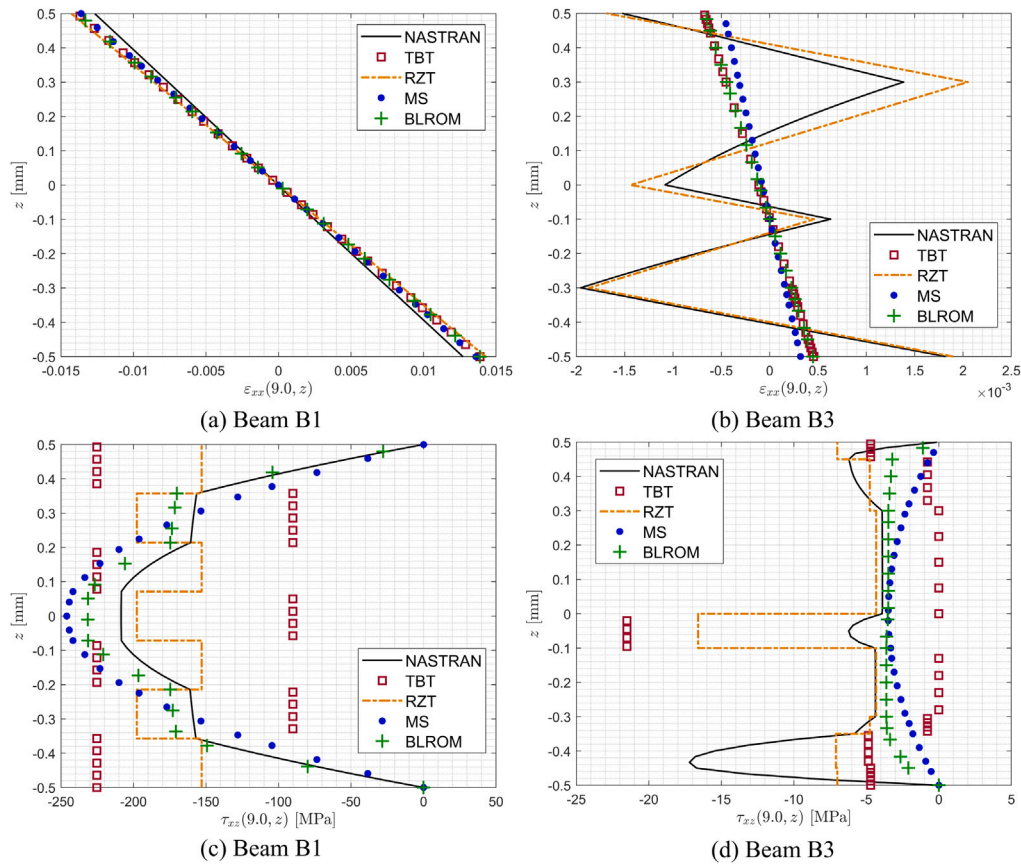


Fig. 17. Axial strain and shear stress distributions in  $x = 9$  mm.

In this sense, the proposed BLROM FE model also adopts the same kinematic variables as the TBT, and it provides an equivalent kinematic 2D response. However, when the latter is well reproduced, this model is the only one able to predict realistic stress distributions in all directions, including the piecewise continuous parabolic shear stress distribution, without requiring a more refined and computationally expensive higher-order model. Furthermore, among the proposed FE models' formulations, the novel BLROM one is the only one that can be used for the analysis of beams with irregular sections cross-sections since the reduction procedure provides the beam stiffness of a longitudinal section regardless of its geometry or lamination. From a computational point of view, the reduction and the condensation procedure can be overtaken by assembling models with elements of the same length, thus reusing the BLROM stiffness matrix for all of them.

In conclusion, the provided numerical results confirm the superiority of the RZT, MS, and BLROM FE models over the TBT one. In addition, the MS and BLROM models that implement the same TBT kinematics are accurate enough for a class of monolithic lamination schemes, and computationally advantageous with respect to high-fidelity FE models. In particular, the BLROM superiority prediction for transverse shear stresses in such cases is preferable over the MS model. Generally, the RZT FE model is suggested when the beam lamination schemes consider layers with strong differences in their transverse shear mechanical properties.

Finally, the results obtained provide a basis for potential meeting points between the presented models, which could lead to further innovations. For example, using the RZT kinematics to define the BLROMs, instead of the TBT, could lead to a much more accurate analysis at the structural level and during laminate evaluation. As shown, structurally, the behaviour of the BLROM models is clearly constrained by the current limitations of the TBT model, which could be improved using

the RZT. In addition, evaluating the degrees of freedom associated with the zig-zag amplitude using a plane stress representation would allow to capture the real stress states arising from the equilibrium itself. Incorporating these features could extend the range of applicability of such models, even for highly heterogeneous/anisotropic and lattice materials in lightweight beams, plates and shell structures, even in the presence of local irregularities.

#### CRediT authorship contribution statement

**Matteo Sorrenti:** Writing – review & editing, Writing – original draft, Visualization, Validation, Software, Methodology, Investigation, Data curation, Conceptualization. **Francesc Turon:** Writing – review & editing, Writing – original draft, Visualization, Validation, Software, Methodology, Investigation, Data curation, Conceptualization. **Fermin Otero:** Writing – review & editing, Validation, Supervision, Resources, Project administration. **Xavier Martinez:** Writing – review & editing, Validation, Supervision, Resources, Project administration. **Marco Gherlone:** Writing – review & editing, Validation, Supervision, Resources, Project administration.

#### Declaration of competing interest

The authors declare that they have no known competing financial interests or personal relationships that could have appeared to influence the work reported in this paper.

#### Acknowledgements

This work has received funding from the European Union's Horizon 2020 research and innovation programme under grant agreement N.101006860 (FIBRE4YARDS project) and under grant agreement



N.952966 (FIBREGY project). In addition, this research work is framed within an FI doctoral grant awarded by the Generalitat de Catalunya, Spain and co-financed jointly with the European Union. These supports are gratefully acknowledged.

## Data availability

Data will be made available on request.

## References

- Abrate, S., Di Sciuva, M., 2017. Equivalent single layer theories for composite and sandwich structures: A review. *Compos. Struct.* 179, 482–494. <http://dx.doi.org/10.1016/j.compstruct.2017.07.090>.
- Ascione, A., Gherlone, M., 2018. Nonlinear static response analysis of sandwich beams using the Refined Zigzag Theory. *J. Sandw. Struct. Mater.* 22, 2250–2286. <http://dx.doi.org/10.1177/1099636218795381>.
- Ascione, A., Gherlone, M., Orifici, A.C., 2022. Nonlinear static analysis of composite beams with piezoelectric actuator patches using the Refined Zigzag Theory. *Compos. Struct.* 282, 1–18. <http://dx.doi.org/10.1016/j.compstruct.2021.115018>.
- Ascione, A., Orifici, A.C., Gherlone, M., 2020. Experimental and numerical investigation of the refined zigzag theory for accurate buckling analysis of highly heterogeneous sandwich beams. *Int. J. Struct. Stab. Dyn.* 20 (7), 1–27. <http://dx.doi.org/10.1142/S0219455420500789>.
- Carrera, E., 2003. Theories and finite elements for multilayered plates and shells: A unified compact formulation with numerical assessment and benchmarking. *Arch. Comput. Methods Eng.* 10 (3), 215–296. <http://dx.doi.org/10.1007/BF02736224>.
- Coenen, E.W., Kouznetsova, V.G., Geers, M.G., 2008. A multi-scale computational strategy for structured thin sheets. *Int. J. Mater. Form.* 1, 61–64. <http://dx.doi.org/10.1007/s12289-008-0044-x>.
- Demasi, L., 2008.  $\infty^3$  Hierarchy plate theories for thick and thin composite plates: The generalized unified formulation. *Compos. Struct.* 84 (3), 256–270. <http://dx.doi.org/10.1016/j.compstruct.2007.08.004>.
- Di Sciuva, M., 1986. Bending, vibration and buckling of simply supported thick multilayered orthotropic plates: An evaluation of a new displacement model. *J. Sound Vib.* 105 (3), 425–442. [http://dx.doi.org/10.1016/0022-460X\(86\)90169-0](http://dx.doi.org/10.1016/0022-460X(86)90169-0).
- Di Sciuva, M., Gherlone, M., Iurlaro, L., Tessler, A., 2015. A class of higher-order  $C^0$  composite and sandwich beam elements based on the Refined Zigzag Theory. *Compos. Struct.* 132, 784–803. <http://dx.doi.org/10.1016/j.compstruct.2015.06.071>.
- Dorduncu, M., 2019. Stress analysis of laminated composite beams using refined zigzag theory and peridynamic differential operator. *Compos. Struct.* 218 (7), 193–203. <http://dx.doi.org/10.1016/j.compstruct.2019.03.035>.
- Geers, M.G., Coenen, E.W., Kouznetsova, V.G., 2007. Multi-scale computational homogenization of structured thin sheets. *Modelling Simul. Mater. Sci. Eng.* 15, S393–S404. <http://dx.doi.org/10.1088/0965-0393/15/4/S06>.
- Gherlone, M., 2013. On the use of zigzag functions in equivalent single layer theories for laminated composite and sandwich beams: A comparative study and some observations on external weak layers. *J. Appl. Mech.* 80 (6), 1–19. <http://dx.doi.org/10.1115/1.4023690>.
- Gherlone, M., Tessler, A., Di Sciuva, M., 2011.  $C^0$  beam elements based on the Refined Zigzag Theory for multilayered composite and sandwich laminates. *Compos. Struct.* 93 (11), 2882–2894. <http://dx.doi.org/10.1016/j.compstruct.2011.05.015>.
- Groh, R.M.J., Weaver, P.M., 2015. On displacement-based and mixed-variational equivalent single layer theories for modelling highly heterogeneous laminated beams. *Int. J. Solids Struct.* 59, 147–170. <http://dx.doi.org/10.1016/j.ijsolstr.2015.01.020>.
- Groh, R.M., Weaver, P.M., Tessler, A., 2015. Application of the Refined Zigzag Theory to the modeling of delaminations in laminated composites. In: *NASA/TM-2015-218808*. pp. 1–22.
- Hasim, K.A., 2018. Isogeometric static analysis of laminated composite plane beams by using refined zigzag theory. *Compos. Struct.* 186, 365–374. <http://dx.doi.org/10.1016/j.compstruct.2017.12.033>.
- Iurlaro, L., Gherlone, M., Di Sciuva, M., Tessler, A., 2013. Assessment of the Refined Zigzag Theory for bending, vibration, and buckling of sandwich plates: a comparative study of different theories. *Compos. Struct.* 106, 777–792. <http://dx.doi.org/10.1016/j.compstruct.2013.07.019>.
- Kefal, A., Tabrizi, I.E., Yildiz, M., Tessler, A., 2021. A smoothed iFEM approach for efficient shape-sensing applications: Numerical and experimental validation on composite structures. *Mech. Syst. Signal Process.* 152, 1–34. <http://dx.doi.org/10.1016/j.ymsp.2020.107486>.
- Kouznetsova, V.G., Geers, M.G., Brekelmans, W.A., 2004. Multi-scale second-order computational homogenization of multi-phase materials: A nested finite element solution strategy. *Comput. Methods Appl. Mech. Engrg.* 193, 5525–5550. <http://dx.doi.org/10.1016/j.cma.2003.12.073>.
- Madabhushi-Raman, P., Davalos, J.F., 1996. Static shear correction factor for laminated rectangular beams. *Compos. Part B: Eng.* 27B (3–4), 285–293. [http://dx.doi.org/10.1016/1359-8368\(95\)00014-3](http://dx.doi.org/10.1016/1359-8368(95)00014-3).
- Malekimoghadam, R., Hosseini, S.A., Icardi, U., 2023. Bending analysis of carbon nanotube coated-fiber multi-scale composite beams using the refined zigzag theory. *Aerosp. Sci. Technol.* 138, 1–24. <http://dx.doi.org/10.1016/j.ast.2023.108328>.
- McCune, R.W., Armstrong, C.G., Robinson, D.J., 2000. Mixed-dimensional coupling in finite element models. *Internat. J. Numer. Methods Engrg.* 49, 725–750. [http://dx.doi.org/10.1002/1097-0207\(20001030\)49:6<725::AID-NME967>3.0.CO;2-W](http://dx.doi.org/10.1002/1097-0207(20001030)49:6<725::AID-NME967>3.0.CO;2-W).
- Monaghan, D.J., Lee, K.Y., Armstrong, C.G., Ou, H., 2000. Mixed dimensional finite element analysis of frame models. In: *10th International Ocean and Polar Engineering Conference*, Vol. 4. pp. 263–269.
- Murakami, H., 1986. Laminated composite plate theory with improved in-plane responses. *J. Appl. Mech.* 53 (3), 661–666. <http://dx.doi.org/10.1115/1.3171828>.
- Noor, A.K., Burton, W.S., 1990. Three-dimensional solutions for antisymmetrically laminated anisotropic plates. *J. Appl. Mech.* 57 (1), 182–188. <http://dx.doi.org/10.1115/1.2888300>.
- Oñate, E., 2013. *Structural Analysis with the Finite Element Method. Linear Statics: Volume 2: Beams, Plates and Shells*. In: *Lecture Notes on Numerical Methods in Engineering and Sciences*, Springer Netherlands.
- Oñate, E., Eijo, A., Oller, S., 2012. Simple and accurate two-noded beam element for composite laminated beams using a refined zigzag theory. *Comput. Methods Appl. Mech. Engrg.* 213–216, 362–382. <http://dx.doi.org/10.1016/j.cma.2011.11.023>.
- Otero, F., Oller, S., Martínez, X., 2018. Multiscale computational homogenization: Review and proposal of a new enhanced-first-order method. *Arch. Comput. Methods Eng.* 25, 479–505. <http://dx.doi.org/10.1007/s11831-016-9205-0>.
- Pagano, N., 1969. Exact solutions for composite laminates in cylindrical bending. *J. Compos. Mater.* 3 (3), 398–411. <http://dx.doi.org/10.1177/002199836900300304>.
- Pagano, N., 1970a. Exact solutions for rectangular bidirectional composites and sandwich plates. *J. Compos. Mater.* 4 (1), 20–34. <http://dx.doi.org/10.1177/002199837000400102>.
- Pagano, N., 1970b. Influence of shear coupling in cylindrical bending of anisotropic laminates. *J. Compos. Mater.* 4 (3), 330–343. <http://dx.doi.org/10.1177/002199837000400305>.
- Reddy, J.N., 1984. A simple higher-order theory for laminated composite plates. *J. Appl. Mech.* 51 (4), 745–752. <http://dx.doi.org/10.1115/1.3167719>.
- Reddy, J.N., 2003. *Mechanics of Laminated Composite Plates and Shells: Theory and Analysis, second ed.* CRC Press.
- Savoia, M., Reddy, J.N., 1992. A variational approach to three-dimensional elasticity solutions of laminated composite plates. *J. Appl. Mech.* 59 (2S), S166–S175. <http://dx.doi.org/10.1115/1.2899483>.
- Tessler, A., 2015. Refined zigzag theory for homogeneous, laminated composite, and sandwich beams derived from Reissner's mixed variational principle. *Meccanica* 50, 2621–2648. <http://dx.doi.org/10.1007/s11012-015-0222-0>.
- Tessler, A., Di Sciuva, M., Gherlone, M., 2007. Refinement of timoshenko beam theory for composite and sandwich beams using zigzag kinematics. In: *NASA/TP-2007-215086*. pp. 1–45.
- Tessler, A., Di Sciuva, M., Gherlone, M., 2010. A consistent refinement of first-order shear-deformation theory for laminated composite and sandwich plates using improved zigzag kinematics. *J. Mech. Mater. Struct.* 5 (2), 341–367. <http://dx.doi.org/10.2140/jomms.2010.5.341>.
- Timoshenko, S., Woinowsky-Krieger, S., 1959. *Theory of Plates and Shells*. McGraw-Hill.
- Turon, F., Otero, F., Ferrer, A., Martínez, X., 2024. Definition of a beam-like reduced order model element by means of a mixed dimensional coupling. *Comput. Struct.* 302, 107466. <http://dx.doi.org/10.1016/J.COMPSTRUC.2024.107466>.
- Washizu, K., 1975. *Variational Methods in Elasticity and Plasticity, second ed.* Pergamon Press.
- Yu, Y., Chan, T., Sun, Z., Li, Z., 2012. Mixed-dimensional consistent coupling by multi-point constraint equations for efficient multi-scale modeling. *Adv. Struct. Eng.* 15 (5), 837–853. <http://dx.doi.org/10.1260/1369-4332.15.5.837>.